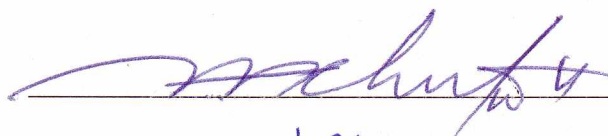


MEASUREMENT OF RHEOLOGICAL AND THERMAL PROPERTIES AND THE  
FREEZE-THAW CHARACTERISTICS OF NANOFUIDS

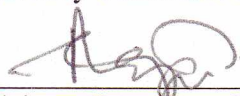
By

Bhaskar C. Sahoo

RECOMMENDED:

  
\_\_\_\_\_

Debendra K Das  
Advisory Committee Co-Chair

  
\_\_\_\_\_

Advisory Committee Co-Chair

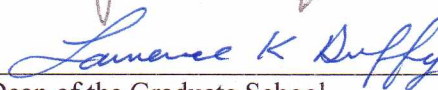
  
\_\_\_\_\_

Chair, Department of Mining and Geological Engineering

APPROVED:

  
\_\_\_\_\_

Dean, College of Engineering and Mines

  
\_\_\_\_\_

Dean of the Graduate School

Dec 8, 2008  
\_\_\_\_\_

Date

MEASUREMENT OF RHEOLOGICAL AND THERMAL PROPERTIES AND THE  
FREEZE-THAW CHARACTERISTICS OF NANOFUIDS

A  
THESIS

Presented to the Faculty  
of the University of Alaska Fairbanks

in Partial Fulfillment of the Requirements  
for the Degree of

MASTER OF SCIENCE

By

Bhaskar C. Sahoo, B.Sc.

Fairbanks, Alaska

December 2008

## ABSTRACT

This research investigates the rheological and thermal properties and the freeze-thaw characteristics of nanofluids. Nanofluids are dispersions of nano-scale particles ( $< 100$  nm) in a base fluid such as water, ethylene glycol, propylene glycol or a mixture of more than one fluid. In cold regions, a mixture of 60% ethylene glycol in water by mass (60:40 EG/W) is normally used as the heat transfer fluid due to its low freezing point. Rheological properties of aluminum oxide nanofluid in the 60:40 EG/W base fluid were investigated and new correlations, expressing viscosity as a function of temperature and particle concentration, were developed. Results from the specific heat experiments on zinc oxide nanofluid in the 60:40 EG/W were compared with available correlations and a new model was developed. The thermal conductivity of silicon dioxide nanofluid in a 60:40 EG/W was measured and compared with existing models, considering the Brownian motion of nanoparticles. A new correlation, expressing thermal conductivity as a function of particle concentration, size, base fluid properties and temperature, was proposed by improving an existing model. Freeze-thaw characteristics of copper oxide nanoparticle dispersions in water were studied for a single freeze-thaw cycle. The freezing rate, agglomeration of nanoparticles and the effect on the freezing point of nanofluid were examined.

## Table of Contents

	Page
Signature Page .....	i
Title Page .....	ii
Abstract .....	iii
Table of Contents .....	iv
List of Figures .....	vi
List of Tables .....	viii
Acknowledgements .....	ix
Chapter 1 Introduction .....	1
1.1 Introduction to Nanofluids .....	1
1.2 Applications of Nanofluids .....	2
1.3 Research Outline and Objectives .....	2
1.3.1 Rheological Properties .....	2
1.3.2 Specific Heat .....	3
1.3.3 Thermal Conductivity .....	3
1.3.4 Freeze-Thaw Characteristics .....	3
1.4 Summary of Thesis Chapters .....	4
References .....	5
Chapter 2 Determination of Rheological Behavior of Aluminum Oxide Nanofluid and Development of New Viscosity Correlations .....	7
2.1 Introduction .....	7
2.2 Experimental Setup and Procedure .....	10
2.3 Results and Discussion .....	11
2.4 Conclusions .....	14
References .....	14
Chapter 3 Experimental Investigation on the Specific Heat of Zinc Oxide Nanofluid .....	22
3.1 Introduction .....	22
3.2 Theory .....	23
3.2.1 Specific Heat Correlations for Nanofluids .....	26
3.3 Experimental Setup and Procedure .....	26

	Page
3.4 Results .....	27
3.4.1 Benchmark Test Case .....	27
3.4.2 ZnO Nanofluid Measurements .....	28
3.4.3 Development of the Specific Heat Correlation .....	28
3.5 Conclusions .....	29
References .....	29
Chapter 4 New Correlations for the Thermal Conductivity of Silicon Dioxide Nanofluid from Experiments .....	34
4.1 Introduction .....	35
4.2 Existing Thermal Conductivity Models .....	36
4.3 Experimental Setup and Procedure .....	37
4.3.1 Development of Calibration Curve .....	38
4.3.2 Uncertainty in Thermal Conductivity Measurements .....	39
4.4 Results and Discussion .....	40
4.4.1 Benchmark Test Case .....	40
4.4.2 Thermal Conductivity of SiO <sub>2</sub> Nanofluid .....	41
4.5 Development of New Correlation .....	42
4.6 Conclusions .....	43
Acknowledgements .....	43
References .....	43
Chapter 5 Freeze-Thaw Characteristics of Water-based Copper Oxide Nanofluid .....	50
5.1 Introduction .....	50
5.2 Experimental Setup and Procedure .....	52
5.3 Results .....	53
5.3.1 Freezing Temperature and rate .....	53
5.3.2 Freeze-Thaw Cycle .....	54
5.3.3 Particle Size Measurement .....	54
5.4 Conclusions .....	54
Acknowledgements .....	55
References .....	55
Chapter 6 Conclusions .....	61

## List of Figures

		Page
Figure 2.1	Experimental setup for viscosity measurement of nanofluids. ....	17
Figure 2.2	Calibration of the viscometer using standard newtonian calibration fluid provided by Brookfield at 25 °C. ....	17
Figure 2.3	Viscosity variation with shear strain rate of Al <sub>2</sub> O <sub>3</sub> nanofluid of 10% concentration at various temperatures (238K to 363K). ....	18
Figure 2.4	Nonnewtonian behavior of Al <sub>2</sub> O <sub>3</sub> nanofluid of 10% volumetric concentration at 243K. ....	18
Figure 2.5	Shear stress versus shear strain rate for a 10% volume concentration of Al <sub>2</sub> O <sub>3</sub> nanofluid at 323K. ....	19
Figure 2.6	Shear stress versus shear strain rate in the higher temperature range (283K to 363K) for the 4% Al <sub>2</sub> O <sub>3</sub> nanofluid. ....	19
Figure 2.7	Variation of viscosity with volumetric concentrations at two distinct temperature regimes. ....	20
Figure 2.8	Experimental and curve-fit viscosity values for various concentrations of Al <sub>2</sub> O <sub>3</sub> nanofluid at low temperatures. ....	21
Figure 2.9	Experimental and curve-fit viscosity values for various concentrations of the Al <sub>2</sub> O <sub>3</sub> nanofluid at high temperatures. ....	21
Figure 3.1	Experimental setup for the specific heat measurement. ....	31
Figure 3.2	Comparison of measured specific heat of water with data from Bejan. ....	31
Figure 3.3	Measured specific heat of ZnO nanofluid as a function of temperature and concentration. ....	32
Figure 3.4	Comparison of experimental specific heat values with Pak and Cho and Buongiorno equations for ZnO nanofluid of 7% concentration. ....	32
Figure 3.5	Variation of specific heat with temperature for 1% and 7% concentrations of ZnO nanofluid. ....	33
Figure 3.6	Specific heat as a function of temperature and concentration. ....	33
Figure 4.1	Experimental setup for thermal conductivity measurements of SiO <sub>2</sub> nanofluid. ....	46
Figure 4.2	Calibration curve for the incidental heat transfer using air as the test fluid. ....	46
Figure 4.3	Benchmark test case to compare measured thermal conductivity values with the ASHRAE data for 60:40 EG/W. ....	47

	Page
Figure 4.4	Variation of thermal conductivity with temperature for several concentrations of SiO <sub>2</sub> nanofluid and comparison with the Hamilton-Crosser (H&C) model. ... 47
Figure 4.5	Variation of thermal conductivity ratio with temperature for different volumetric concentrations of SiO <sub>2</sub> nanofluid. .... 48
Figure 4.6	Variation of thermal conductivity ratio with concentration for SiO <sub>2</sub> nanofluid from experiment and Hamilton-Crosser correlation (H&C). .... 48
Figure 4.7	Comparison of experimental thermal conductivity with predicted values for SiO <sub>2</sub> nanofluid obtained from the new correlations. .... 49
Figure 5.1	Experimental setup to study the freeze-thaw characteristics of the CuO nanofluid. .... 58
Figure 5.2	Freezing characteristic curves for water and CuO nanofluid at location B2. .... 58
Figure 5.3	Freezing characteristic curve of deionized water. .... 59
Figure 5.4	Freeze-Thaw characteristic curve of CuO nanofluid of 1% volumetric concentration. .... 59
Figure 5.5	Freeze-Thaw characteristic curve of CuO nanofluid of 5% volumetric concentration. .... 60

**List of Tables**

	Page
Table 2.1 Viscosity curve-fit parameters for the low and high temperature regimes. ....	16
Table 5.1 Average particle size distribution for the CuO nanofluid before and after freezing. ....	57

## ACKNOWLEDGEMENTS

I gratefully acknowledge the incessant support of my thesis advisor Dr. Debendra K. Das, for the successful completion of this thesis. His experienced mentoring and guidance added great value to my scholarly and personal achievements. I would like to thank my committee members Dr. Rajive Ganguli and Dr. Godwin Chukwu for their timely advice and suggestions in improving the research.

I appreciate the help of Dr. Rorik Peterson and Dr. Thomas Trainor in the experimental aspects of this research.

My sincere appreciation goes to my wife Rupali, who spent sleepless nights looking at the computer screen and proof-reading my manuscripts for errors. Also, her patience and culinary expertise were instrumental in the smooth completion of this work. Finally, I would like to thank my family and friends for their encouragement and good wishes for my career.

## CHAPTER 1

### INTRODUCTION

#### 1.1 Introduction to Nanofluids

Nanofluids are dispersions of nano-scale particles (e.g. copper, alumina, silica and zinc oxide etc.) in a base fluid such as water, ethylene glycol, propylene glycol, olefin, oil, or a mixture of more than one fluid. For effective heat transfer, it is preferred that the nanoparticle size be smaller than 100 nm. In cold regions, a 50% or 60% mixture of ethylene or propylene glycol (by mass) in water are normally used for heat transfer since their freezing points are much lower than water. This base fluid is referred to as 60:40 EG/W in this research.

Particles, due to their higher thermal conductivity, are known to augment thermal performance of the heat transfer fluids when dispersed in the base fluids. Thermal enhancement is further achieved due to an increase in the effective surface area of the particles in contact with the base fluid. In this context, it is observed that dispersions of nanoparticles exhibit better thermal properties than micro or bigger particles due to the greater surface area of contact of the former. Also, Boutin [1] found that whereas nearly 20% of the atoms participating in heat transfer reside near the surface of the nanoparticles, in microparticles, most of the atoms remain far inside the surface where heat transfer takes place. For example, from an experimental study, Eastman et al. [2] have shown that a 0.3% volumetric concentration of copper nanoparticles in ethylene glycol resulted in a 40% increase in thermal conductivity of the base fluid. Pak and Cho [3], from studies on aluminum oxide ( $\text{Al}_2\text{O}_3$ )-water nanofluid found that a 2.78% particle concentration enhanced the convective heat transfer coefficient by 75%. Moreover, micro-particles are prone to gravitational settling, agglomeration and in many heat transfer applications cause erosion to the walls of flow channels. With the burgeoning energy crisis gripping the world, it is no surprise that research in nanofluids has been much in demand in recent years.

Nanofluid research is a relatively new field which is expanding very rapidly. Knowledge of thermal and rheological properties of nanofluids is necessary to evaluate the viability of using nanofluids in practical applications. Rheological property is necessary to determine the pumping power required to circulate the nanofluid. Such properties are still being investigated by researchers. Subsequent chapters in this thesis aim at exploring the rheological (stress-strain behavior and viscosity), thermal (specific heat and thermal conductivity) and freeze-thaw

characteristics of some commonly available nanofluids. The importance of these properties is outlined in Section 1.3.

Presently, the major challenge in nanofluid research is to achieve a stable dispersion, which ensures consistent thermal properties in time.

## **1.2 Applications of Nanofluids**

Nanofluids are potential candidates in heat transfer applications in many fields of research. Some of such areas include computer engineering (cooling micro-chips), petroleum industry (as thermal stimulant fluid in thawing gas hydrates), thermal engineering (building heating, heat exchangers) and automobile industry (vehicle radiators). In all such applications, the reduction of size in heat exchangers and the volume reduction of the circulating fluids could result in great material and energy savings and pumping power.

Nanofluids, due to their unique spreading behavior on solid surfaces, can be used with surfactant micelles for environmental and geotechnical applications such as soil remediation, oily soil removal, lubrication and enhanced oil recovery [4].

## **1.3 Research Outline and Objectives**

As described earlier, the goal of this research is to investigate rheological and thermal properties of commonly used nanofluids with different nanoparticles (metallic, non-metallic) and base fluids (60:40 EG/W and 50:50 EG/W, water). This work also attempts to study the freeze-thaw characteristics of nanofluids for effective thermal applications in cold climates.

### *1.3.1 Rheological Properties*

Convective heat transfer coefficients of fluids and pumping power requirements depend strongly on the Reynolds and Prandtl numbers, which in turn, are highly influenced by viscosity. Thus, accurate determination of viscosity of fluids is very important in thermal applications. Xuan and Li [5] have reported conspicuous enhancement of the heat transfer coefficient in nanofluids of low particle concentration without much penalty in pressure loss. Namburu et al. [6] developed a viscosity correlation for  $\text{Al}_2\text{O}_3$  nanofluid in EG/W in the temperature range of  $-35^\circ\text{C}$  to  $50^\circ\text{C}$ . However, in building heating applications fluid temperatures as high as  $90^\circ\text{C}$  are employed and hence, their correlation is inadequate for building heating systems. This motivated

the present research for viscosity measurements of  $\text{Al}_2\text{O}_3$  nanofluids with different volumetric concentrations and at higher temperatures.

### *1.3.2 Specific Heat*

The Prandtl number is a function of thermo-physical properties (e.g. specific heat) and pivotal in the determination of convective heat transfer coefficients. The total heat transfer rate through the wall of a heat exchanger flow passage (e.g. an automobile radiator or building heating coil) depends strongly on the specific heat of the fluid. Thermal diffusivity, another important parameter in heat transfer, is a function of specific heat [7]. In order to determine how fast heat will diffuse through the nanofluid, this parameter must be known accurately. Therefore, it is apparent that accurate determination of specific heat is very important in the evaluation of nanofluid thermal performance. Experimental data on the specific heat of nanofluids is very limited. Only Zhou and Ni [8] have reported specific heat measurements of water-based  $\text{Al}_2\text{O}_3$  nanofluid and no data with 60:40 EG/W base fluid is available. Therefore, the second objective of this research is to measure the specific heat of a nanofluid. A dispersion of zinc oxide (ZnO) nanoparticles in 60:40 EG/W is selected, as the data on such nanofluids is not available.

### *1.3.3 Thermal Conductivity*

Since for a given Nusselt number, the convective heat transfer coefficient of a fluid is directly proportional to its thermal conductivity, its accurate determination is very important in evaluating the thermal performance of nanofluids. Lee et al. [9] reported an enhancement of over 20% in thermal conductivity of ethylene glycol when copper oxide (CuO) nanoparticles of 4% volumetric concentration were suspended in it. Much of the thermal conductivity studies have been reported on metallic nanoparticles. Therefore, the third objective of this research is to experimentally investigate the thermal conductivity of silicon dioxide nanoparticles dispersed in 60:40 EG/W.

### *1.3.4 Freeze-Thaw Characteristics*

As mentioned earlier, the main challenge in nanofluids to become successful as efficient heat transfer fluids, is to achieve stable suspensions over a period of time. Nanoparticles in such fluids, when subjected to freeze-thaw, tend to agglomerate, resulting in bigger size particles. Agglomeration leads to phase separation and subsequently, thermal properties of the nanofluids

change constantly [10] as the nanoparticles gradually separate from the base fluid. Also, it is well known that particle size significantly affects the thermal performance of nanofluids [11]. Smaller nanoparticle size results in greater surface area and hence better heat transfer characteristics. In cold region applications, nanofluids may undergo one or more freeze-thaw cycles and it is desirable to study the effect of such cycles on agglomeration in terms of particle size. Therefore, the main objective of this research is to study the freeze-thaw characteristics of CuO nanoparticles dispersed in water.

#### **1.4 Summary of Thesis Chapters**

This thesis is divided into six chapters and is written in manuscript format. Individual chapters coherently address specific issues in nanofluid research and contain complete references to related work.

Chapter-1 provides background and general introduction on nanofluids. It includes the motivation behind this research, applications of nanofluids and objectives of the research. It also gives a summary of Chapter-2 through Chapter-5.

Chapter-2 : Rheological characteristics of  $\text{Al}_2\text{O}_3$  nanofluids with average particle size (APS) of 53nm and concentrations ranging from 1 to 10% in a 60:40 EG/W base fluid were investigated over a temperature range of  $-35^\circ\text{C}$  to  $90^\circ\text{C}$ . From this investigation, two new correlations have been developed, expressing viscosity as a function of temperature and particle volumetric concentration.

Chapter-3 : Specific heat of ZnO nanoparticles dispersions (70nm APS) in a 60:40 EG/W base fluid is experimentally determined and the data is compared with other available correlations. From the experimental data a new correlation was developed for the specific heat of ZnO nanofluid.

Chapter-4 : Thermal conductivity of  $\text{SiO}_2$  nanoparticles dispersions (77nm APS) in a 60:40 EG/W base fluid is experimentally determined and the data is compared with existing models considering the Brownian motion of nanoparticles. A new correlation expressing thermal conductivity as a function of particle concentration and temperature was proposed by improving the Koo and Kleinstreuer [12] model.

Chapter-5 : Freeze-thaw characteristics of a water-based CuO nanofluid (30nm APS) is studied. Freeze-thaw characteristic curves of two volumetric concentrations (1% and 5%) and the base fluid (water) are experimentally determined for a single freeze-thaw cycle. The

agglomeration effect of freezing, in terms of average particle size distribution, is studied for both the concentrations. Also, the effect of adding nanoparticles in water in lowering its freezing point is examined.

Chapter-6 provides conclusions and a summary of the research documented in Chapter-2 through Chapter-5.

## References

- [1]. Boutin, C. (2001). *Taking the heat off: Nanofluids promise efficient heat transfer*. Available: <http://www.anl.gov/OPA/logos19-2/nanofluids01.htm>. Last accessed October 10, 2005.
- [2]. Eastman, J.A., Choi, S.U.S., Li, S., Yu, W. and Thompson, L.J. (2001). Anomalous increased effective thermal conductivities of ethylene glycol based nanofluids containing copper nanoparticles. *Applied Physics Letters*. 78 (6): 718–720.
- [3]. Pak, B.C. and Cho, Y.L. (1998). Hydrodynamics and heat transfer study of dispersed fluids with submicron metallic oxide particles. *Experimental Heat Transfer*. 11: 151–170.
- [4]. Wasan, D. T. and Nikolov, A. D. (2003). Spreading of Nanofluids on Solids. *Nature*. 423: 156–159.
- [5]. Xuan, Y. and Li, Q. (2003). Investigation on convective heat transfer and flow features of nanofluids. *Journal of Heat Transfer*. 125: 151–155.
- [6]. Namburu, P.K., Das, D.K., Tanguturi, K.M., and Vajjha, R.S. (2008). Numerical Study of Turbulent Flow and Heat Transfer Characteristics of Nanofluids Considering Variable Properties. *Intl Jour. of Thermal Sci.* (In Press), doi: 10.1016/j.ijthermalsci.2008.01.001.
- [7]. White, F.M. (1988). *Heat and Mass Transfer*. New York : Addison Wesley Publishing Co.
- [8]. Zhou, S.Q. and Ni, R. (2008). Measurement of the specific heat capacity of water-based Al<sub>2</sub>O<sub>3</sub> nanofluid. *Applied Physics Letters*, 92(2): Art. No. 093123.
- [9]. S. Lee, Choi, S.U.S., Li, S., Eastman, J. (1999). Measuring thermal conductivity of fluids containing oxide nanoparticles. *Jour. Heat Transfer*. 121: 280-289.
- [10]. Hong, H. and Marquis, F.D. S. (2007). *Carbon nanoparticle-containing hydrophilic nanofluid*. Available: <http://www.freepatentsonline.com/20070158610.html>. Last accessed 1 October 2008.

- [11]. Chon, H.C., Kihm, K.D., Lee, S.P. and Choi, S.U.S. (2005). Empirical correlation finding the role of temperature and particle size for nanofluid ( $\text{Al}_2\text{O}_3$ ) thermal conductivity enhancement. *Appl. Phys. Lett.* 87, 153107: 1-3.
- [12]. Koo, J. and Kleinstreuer, C. (2004). A new thermal conductivity model for nanofluids. *Jour. Nanoparticle Research*. 6: 577-588.

## CHAPTER 2

### DETERMINATION OF RHEOLOGICAL BEHAVIOR OF ALUMINUM OXIDE NANOFUID AND DEVELOPMENT OF NEW VISCOSITY CORRELATIONS<sup>1</sup>

#### Abstract

Experimental investigations have been carried out to study the rheological behavior of aluminum oxide nanofluid. Nanoparticles with average particle size of 53 nm were dispersed in a base fluid of 60% (by mass) of ethylene glycol and water. Nanofluids of volumetric concentrations 1 to 10% were tested for determining the viscous properties. It was found that this nanofluid behaved as nonnewtonian at lower temperatures (-35°C to 0°C) and newtonian at higher temperatures (0°C to 90°C). The data showed that the viscosity increases with an increase in concentration and decreases with increase in temperature. Two new correlations were developed expressing viscosity as a function of temperature and concentration.

**Keywords:** nanofluids, aluminum oxide, viscosity, ethylene glycol, particle concentration, temperature dependency.

#### 2.1 Introduction

Nanofluids are mixtures of solid nanoparticles with average particle size smaller than 100nm dispersed in base fluids such as water, ethylene glycol or propylene glycol. Research on nanofluids has received great attention in the last decade due to the prospect of enhanced thermal properties. For example, Eastman et al. (2001) have reported a 40% increase in thermal conductivity of ethylene glycol when copper nanoparticles of 3% volumetric concentration were added to it. Pak and Cho (1998) have shown that at a fixed Reynolds number, convective heat transfer coefficient of an Al<sub>2</sub>O<sub>3</sub> nanofluid of volume concentration 2.78% increases by 75%. Such results have motivated researchers to explore the thermal and rheological properties of nanofluids.

Heating industrial and residential buildings in cold regions requires a great deal of energy. In such severe cold climatic conditions, aqueous mixtures of ethylene or propylene glycol in different volumetric concentrations are typically used to lower the freezing point of the heat

---

<sup>1</sup> Sahoo, B.C., R.S. Vajjha, R. Ganguli, G.A. Chukwu and D.K. Das. 2008. Determination of Rheological Behavior of Aluminum Oxide Nanofluid and Development of New Viscosity Correlations. Accepted for publication in Petroleum Science and Technology.

transfer medium [McQuiston et al., 2000]. Such heat transfer fluids, which can operate effectively at very low temperatures, are used in building heating systems, automobiles and heat exchangers in industries. It is found that at low temperatures, aqueous mixtures of ethylene glycol have better heat transfer characteristics than propylene glycol [ASHRAE, 2005] and an aqueous mixture of 60% ethylene glycol (by mass), referred to as 60:40 EG/W in this paper provides the freeze protection down to very low temperatures. For this reason, this fluid is most commonly used in the sub-arctic and arctic regions of the world.

Since a very limited amount of data is available on the EG/W based nanofluids, we studied the rheological characteristics of aluminum oxide ( $\text{Al}_2\text{O}_3$ ) nanofluids. This research will help understand the viscous behavior of nanofluids, which is crucial for successful application of nanofluids in cold regions. Xuan and Li (2003) have reported conspicuous enhancement of the heat transfer coefficient in nanofluids of low particle concentration without much penalty in pressure loss. Namburu et al. (2008) developed a viscosity correlation for  $\text{Al}_2\text{O}_3$  nanofluid in EG/W in the temperature range of  $-35^\circ\text{C}$  to  $50^\circ\text{C}$ . However, in building heating applications fluid temperatures as high as  $90^\circ\text{C}$  are employed. Therefore, their correlation is inadequate for building heating systems, which motivated the present research for viscosity measurements of  $\text{Al}_2\text{O}_3$  nanofluids with different volumetric concentrations and at higher temperatures. Rheological characteristics of  $\text{Al}_2\text{O}_3$  nanofluids of concentrations ranging from 1 to 10% in a 60:40 EG/W base fluid were investigated over a temperature range of  $-35^\circ\text{C}$  to  $90^\circ\text{C}$  for their effective usage in cold regions.

Pumping power requirements and convective heat transfer coefficients of fluids depend strongly on the Reynolds and Prandtl numbers, which in turn, are highly influenced by viscosity. Thus, accurate determination of viscosity of fluids is very important in thermal applications. However, research on nanofluid viscosity at very low temperatures encountered in sub-arctic and arctic regions are extremely limited. Correlations for nanofluid viscosity attempt to express viscosity as a function of temperature and particle volumetric concentration. Some of the presently available correlations are discussed below.

For suspensions with particle concentrations below 5% Einstein (1956) proposed a viscosity correlation

$$\mu_s = \mu_f \left( 1 + \frac{5}{2} \phi \right) \quad (1)$$

Another correlation for higher concentrations was given by Brinkman (1952)

$$\mu_s = \mu_f \frac{1}{(1-\phi)^{2.5}} \quad (2)$$

Similar correlation relating viscosity with concentration was proposed by Bicerano et al. (1999)

$$\mu_s = \mu_f (1 + \eta\phi + k_H\phi^2 + \dots) \quad (3)$$

where  $\eta$  is the virial coefficient and  $k_H$  is Huggins coefficient.

In Eqs. (1)-(3)  $\mu_s$  = suspension viscosity,  $\mu_f$  = viscosity of base fluid and  $\phi$  = particle volumetric concentration.

It should be noted that in all the three correlations mentioned above, the suspension viscosity is expressed as a function of particle concentration and temperature does not appear exclusively as a variable. However, it is well known that viscosity of liquids is a strong function of temperature. White (1991) proposed a correlation including temperature dependence of viscosity for pure fluids ( $\mu_f$ )

$$\ln \frac{\mu_f}{\mu_0} \approx a + b \left( \frac{T_0}{T} \right) + c \left( \frac{T_0}{T} \right)^2 \quad (4)$$

In Eq. (4)  $\mu_0$ ,  $T_0$  are reference viscosity and temperature (absolute), respectively. The parameters  $a$ ,  $b$  and  $c$  are dimensionless curve-fit constants, which depend on the type of fluid considered. For example, in the case of pure water  $a = -2.10$ ,  $b = -4.45$  and  $c = 6.55$ .

The Andrade's equation cited by Reid et al. (1987) is an exponential correlation between the viscosity of fluids and their temperature

$$\mu_f = Ae^{B/T} \quad (5)$$

where  $A$  and  $B$  are curve-fit parameters.

Yaws presented a viscosity correlation valid for many industrially important chemical liquids

$$\log(\mu_f) = A + \frac{B}{T} + CT + DT^2 \quad (6)$$

where,  $A$ ,  $B$ ,  $C$  and  $D$  are curve-fit parameters unique to a liquid.

In a study of copper oxide (CuO) nanoparticles suspended in water and for a temperature range of 5–50°C, Kulkarni et al. (2006) proposed a correlation

$$\ln(\mu_{nf}) = A \left( \frac{1}{T} \right) - B \quad (7)$$

In Eq. (7),  $\mu_{nf}$  is the nanofluid viscosity and curve-fit parameters  $A$  and  $B$  are expressed as functions of the nanoparticle concentration ( $\phi$ ). Since the above correlation was developed for an aqueous base fluid, it is not applicable at sub-zero temperatures.

Namburu et al. (2008) developed a viscosity correlation for various concentrations (1-10%) of  $\text{Al}_2\text{O}_3$  nanofluids in a temperature range of  $-35^\circ\text{C}$  to  $50^\circ\text{C}$  for a 60:40 EG/W base fluid

$$\log(\mu_{nf}) = Ae^{BT} \quad (8)$$

where  $A$  and  $B$  are expressed as polynomial functions in nanoparticle concentration ( $\phi$ ).

However, this correlation is not applicable for temperatures above  $50^\circ\text{C}$ . Upon careful inspection it was found that this correlation may have deviations in the range of  $\pm 30\%$  from the measured viscosity values. Therefore, the present study aimed at developing new correlations for a broader temperature range extending up to  $90^\circ\text{C}$ , which is typical of fluids used in building heating. This will help develop the next generation of heat transfer fluids applicable in cold regions.

## 2.2 Experimental Setup and Procedure

The original nanofluid procured from Alfa Aesar (2007) is a 50% (by mass) of  $\text{Al}_2\text{O}_3$  nanoparticle dispersion in water. The average particle size is 53nm and the particle density is 3.6 gm/cc. Nanofluid samples of different particle volumetric concentrations (1, 2, 4, 6, 8 and 10%) were prepared by adding exact amount of ethylene glycol and water to the original nanofluid with a precision mass balance of 0.1mg accuracy. In the newly prepared samples, 60:40 EG/W was the base fluid. Subsequently, the sample was placed in an ultrasonic agitator for a minimum of 90 minutes to ensure uniform dispersion of the nanoparticles.

The experimental setup for measuring the rheological property of  $\text{Al}_2\text{O}_3$  nanofluids is shown in Figure 2.1. The setup consists of an LV DV-II+ Brookfield programmable viscometer (Brookfield, 1999) and a Julabo temperature-controlled bath. For different spindle combinations the viscometer has the ability to measure viscosities in the range of 1.5–30,000 cP [1 cP = 1 mPa.s]. The test fluid, whose viscosity is to be measured, is placed inside the sample chamber. The motor of the viscometer rotates a spindle immersed in the test fluid. Viscous drag of the fluid against the spindle due to rotation is measured by a sensitive calibrated spring attached to the spindle. Temperature of the test fluid is controlled between  $-35^\circ\text{C}$  to  $90^\circ\text{C}$  by a programmable computer connected to the Julabo temperature bath. During viscosity measurements, sample

temperature is recorded by a Resistance Temperature Detector (RTD) sensor attached to the sample chamber. For a specified spindle type, the viscosity measurements are more accurate when rotational speed combinations produce a torque above 10%. Computer-1 connected to the viscometer, records the data through the WINGATHER<sup>®</sup> software (Brookfield, 1999), which includes rotational speed of the spindle (RPM), torque (%), viscosity (cP), shear stress (dyne/cm<sup>2</sup>), shear strain rate (1/s), temperature (°C) and time duration for which the readings are taken.

**Calibration:** Relationship between the shear strain rate ( $\dot{\gamma}$ ) and shear stress ( $\tau$ ) for a newtonian fluid is given by the equation

$$\tau = \mu\dot{\gamma} \quad (9)$$

where  $\mu$  is the coefficient of viscosity.

To verify the accuracy of our experimental setup and procedure, viscosity of the Brookfield Calibration Fluid 10, which is newtonian, was measured. The shear stress and shear strain rates at 13 different rotational speeds of the spindle within the torque limit of 10% - 90% (as recommended by the Brookfield LV-II viscometer manual, 1999) were recorded and the results are shown in Figure 2.2. A straight line passing through the origin fits the stress-strain rate data very well and therefore, clearly exhibits newtonian behavior. From the slope of the stress-strain rate curve a viscosity value of 9.44cP was recorded using the WINGATHER<sup>®</sup> software. This measured value is within a very acceptable error limit of 2.6% of the true viscosity provided by Brookfield Engineering Laboratories.

After calibration of the apparatus and qualifying the procedure with the benchmark test case, the experimental setup was used for measuring the viscosity of the aluminum oxide nanofluid of various particle volumetric concentrations. For the experiments, SC4-18 spindle was used. The rotational speed used in this study ranged from 0-200 RPM. Viscosity measurements were taken at intervals of 10°C. Sufficient time (a minimum of 30 minutes) was given for temperature to stabilize and thus, each viscosity measurement was taken under thermal equilibrium.

### 2.3 Results and Discussion

Namburu et al. (2008) had collected viscosity data of Al<sub>2</sub>O<sub>3</sub> nanofluid of various concentrations in the temperature range of -35°C to 50°C. In the present research, viscosity

measurements were extended to 90°C and new correlations were developed, which gave improved accuracy and applicability over a broader range of temperatures.

It is crucial to determine whether the nanofluid displays newtonian or nonnewtonian behavior with variation of particle concentration and temperature. Figure 3 displays the viscosity versus shear strain rate for Al<sub>2</sub>O<sub>3</sub> nanofluid of 10% volumetric concentration over a temperature 238K (-35°C) to 363K (90°C). Because the viscosity changes with shear strain rate from 238K to 273K, the nanofluid behaves as a nonnewtonian fluid in this temperature range. However, beyond 273K, the viscosity remains constant for all values of shear strain rate indicating a newtonian behavior.

Plots such as Figure 2.3 were generated for all concentrations and nonnewtonian behavior was observed in the lower temperature range (238K to 273K). However, in the higher temperature range (273K to 363K) the fluid behaved as newtonian.

In order to characterize the nonnewtonian behavior, the stress-strain data in the lower temperature range were plotted to ascertain the rheological behavior of the nanofluid. The shear stress ( $\tau$ ) versus shear rate ( $\dot{\gamma}$ ) plot (Figure 2.4) of the nanofluid with 10% concentration at 243K shows that the data fits quite well with the characteristic of a Bingham plastic. It is observed that a yield stress ( $\tau_y$ ) is necessary before the fluid starts deforming. The equation for the straight line shown in Figure 2.4 is

$$\tau = \tau_y + \mu\dot{\gamma} \quad (10)$$

A yield stress  $\tau_y$  of 2.0161 dyne/cm<sup>2</sup> and a viscosity  $\mu$  of 238.08 cP were observed in this case.

Therefore, in the lower temperature range the Al<sub>2</sub>O<sub>3</sub> nanofluid behaves as a Bingham plastic. This observation is in agreement with the conclusions made by Macosko and Mendes (1996), where they specify that concentrated suspension of solid particles in newtonian liquids show a yield stress followed by nearly newtonian flow. Similar plots as Figure 2.4 were created for concentrations of 1, 2, 4, 6 and 8% and the yield stress (the intercept in Figure 2.4) values increased with concentration and decreased with temperature.

The results of viscosity measurements in the higher temperature range, where the nanofluid is newtonian, are discussed next. The stress-strain behavior of a 10% concentration Al<sub>2</sub>O<sub>3</sub> nanofluid at 323K shows a newtonian behavior (Figure 2.5).

Following this, the stress-strain curves were plotted (Figure 2.6) for a nanofluid with 4% concentration tested in the higher temperature range. It is confirmed that in this temperature

regime, the nanofluid exhibits newtonian behavior. Similar behavior was observed in case of the other concentrations tested.

The influence of particle concentration on viscosity in both the temperature regimes is displayed in Figure 2.7. It shows that the  $\text{Al}_2\text{O}_3$  nanofluid viscosity increases with an increase in concentration and it decreases with an increase in temperature. The upper plot shows viscosity variation in the lower temperature regime and the lower plot shows the same for the higher temperature regime.

Analysis of the rheological data compiled in Figure 2.3 through 2.7 confirmed distinct behaviors in two regimes: one in the lower temperature range and the other in the higher temperature range. Therefore, two corresponding correlations must be developed to correctly describe the viscous behavior of the  $\text{Al}_2\text{O}_3$  nanofluid.

Correlations developed by Namburu et al. (2008), Kulkarni et al. (2006), Yaws (1997), White (1991) and Andrade's equation in Reid et al. (1987), were tested to fit the experimental data. However, it was found that none of these correlations fit the data properly. Therefore, by careful statistical analyses an exponential model was derived using the LABFIT<sup>®</sup> (2008) software to arrive at the best-fit correlations for the experimental data. While fitting the data, temperature and concentration were taken as the independent (predictor) variables and viscosity was taken as the dependent (response) variable. This equation fits the data with  $R^2 > 0.99$  in both the low and high temperature regimes

$$\mu_{nf} = Ae^{(B/T+C\phi)} \quad (11)$$

where  $\mu_{nf}$  is viscosity of the  $\text{Al}_2\text{O}_3$  nanofluid in centipoise (cP),  $T$  is the absolute temperature in  $K$ . The curve-fit parameters  $A$ ,  $B$  and  $C$  are characteristics of the nanofluid for the given temperature regimes (238K-273K) and (273K-363K). In Eq. (11), particle concentration ( $\phi$ ) is expressed in percent volume of particles in the base fluid and varies from 0 to 10. Table-2.1 summarizes the curve-fit parameters for the lower and higher temperature regimes. Viscosity of the nanofluids for different particle concentrations and temperatures were computed from the correlation given by Eq (11). The experimental and curve-fitted viscosity values are plotted against temperature for both the low (Figure 2.8) and high (Figure 2.9) temperature regimes.

Unlike the correlations proposed by Kulkarni et al. (2006) and Namburu et al. (2008), where the curve-fit coefficients are dependent on the particle concentration  $\phi$ , the new correlations [Eq. (11)] contains constants  $A$ ,  $B$  and  $C$ , which are independent of  $\phi$ . In Eq. (11),

both  $T$  and  $\phi$  appear in a form similar to the well-known Andrade's equation for viscosity. Except for high temperatures (353K and 363K), the experimental and curve-fit values agree within a deviation of  $\pm 10\%$ . Therefore, the correlations are much simpler and predict viscosity better over a wider range of temperatures. At 363K, the deviation is higher and is attributed to the operational limitation of the viscometer, whose lower limit is 1.5 cP. This error can be reduced by using a more precise viscometer (e.g. the cone-plate viscometer) to obtain very low viscosity values at higher temperatures.

## 2.4 Conclusions

1. Aluminum oxide nanoparticles in a 60:40 EG/W base fluid exhibit a nonnewtonian behavior at a lower temperature range of 238K to 273K for all particle concentrations. It behaves as a Bingham plastic with small yield stress, which decreases with decrease in volumetric concentration and increase in fluid temperature.
2. In the higher temperature range (273K to 363K) the nanofluid behaves as a newtonian fluid.
3. The viscosity of nanofluids increases with an increase in particle concentration. For example, viscosity of 10% concentration aluminum oxide nanofluid is about 4 times the value of that of the base fluid at 238K.
4. Two empirical correlations have been developed to accurately determine the viscosity for two temperature regimes. In both regimes, as the temperature increases, nanofluid viscosity decreases exponentially.
5. The new empirical correlations expressed by Eq. (11) for the  $\text{Al}_2\text{O}_3$  nanoparticles in a 60:40 EG/W base fluid exhibit an exponential relationship between the viscosity and volume concentration.

## References

- Alfa Aesar. 2008. Available: <http://www.alfaesar.com>. Last accessed April 15, 2008.
- ASHRAE. 2005. *ASHRAE Handbook – Fundamentals (SI)*. American Society of Heating, Refrigerating and Air-Conditioning Engineers Inc., Atlanta. 21.4-21.7.
- Bicerano, J., Douglas, J.F. and Brune, D.A. 1999. Model for the viscosity of particle dispersions. *Journal of Macromolecular Science Review*. C39: 561–642.
- Brinkman, H.C. 1952. The viscosity of concentrated suspensions and solutions. *Journal Chemistry Physics*. 20: 571–581.

- Brookfield. 1999. *DV-II+ Programmable Viscometer Manual, No. M/97-164-D1000*. Brookfield Engineering Laboratories Inc., Massachusetts.
- Eastman, J.A., Choi, S.U.S., Li, S., Yu, W. and Thompson, L.J. 2001. Anomalously increased effective thermal conductivities of ethylene glycol based nanofluids containing copper nanoparticles. *Applied Physics Letters*. 78 (6): 718–720.
- Einstein, A. 1956. *Investigations on the Theory of the Brownian Movement*. Dover Publications, New York.
- Kulkarni, D.P., Das, D.K. and Chukwu, G.A. 2006. Temperature dependent rheological property of copper oxide nanoparticles suspension. *Jour. Nanosc. and Nanotechnology*. 6: 1150–1154.
- Macosko, C.W. and Mendes, P.R.S. 1996. Fluid Mechanics Measurements in Non-Newtonian Fluids. In : Goldstein, R.J. (Ed). *Fluid Mechanics Measurements*. Taylor and Francis, Washington, DC.
- McQuiston, F.C., Parker, J.D. and Spitler, J.D. 2000. *Heating Ventilating and Air-Conditioning*. John Wiley & Sons Inc., New York.
- Namburu, P.K., Das, D.K., Tanguturi, K.M., and Vajjha, R.S. 2008. Numerical Study of Turbulent Flow and Heat Transfer Characteristics of Nanofluids Considering Variable Properties. *International Journal of Thermal Sci.* doi: 10.1016/j.ijthermalsci.2008.01.001
- Pak, B.C. and Cho, Y.L. 1998. Hydrodynamics and heat transfer study of dispersed fluids with submicron metallic oxide particles. *Experimental Heat Transfer*. 11: 151–170.
- Reid, R.C., Prausnitz, J.M., and Sherwood, T.K. 1987. *The properties of Gases and Liquids*, 4<sup>th</sup> ed. McGraw-Hill, New York.
- Silva, Wilton P. and Silva, Cleide M.D.P.S. 2008. LAB Fit Curve Fitting Software (Nonlinear Regression and Treatment of Data Program) V 7.2.37 (1999-2007), Available: [www.labfit.net](http://www.labfit.net). Date of access: April 15, 2008.
- White, F.M. 1991. *Viscous Fluid Flow*. McGraw Hill, New York.
- Xuan, Y. and Li, Q. 2003. Investigation on convective heat transfer and flow features of nanofluids. *Journal of Heat Transfer*. 125: 151–155.
- Yaws, C.L. 1977. *Physical Properties - A Guide to the Physical, Thermodynamic and Transport Property Data of Industrially Important Chemical Compounds*, McGraw-Hill, New York.

Table 2.1 Viscosity curve-fit parameters for the low and high temperature regimes.

Curve-fit parameters	Low Temperature Regime (238K – 273K)	High Temperature Regime (273K – 363K)
$A$	$1.2200 \times 10^{-6}$	$2.3920 \times 10^{-4}$
$B$	4285	2903
$C$	0.1448	0.1265
$R^2$	0.9984	0.9958

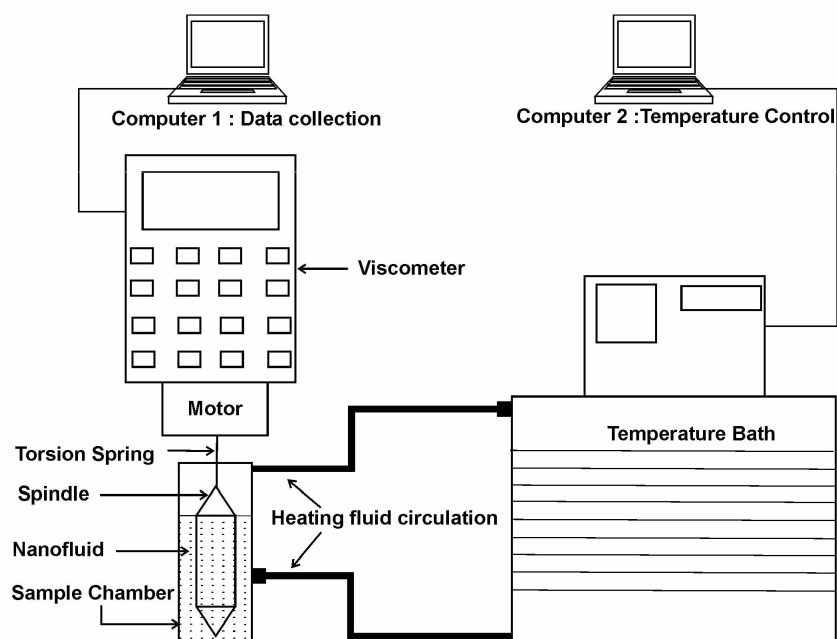


Figure 2.1 Experimental setup for viscosity measurement of nanofluids.

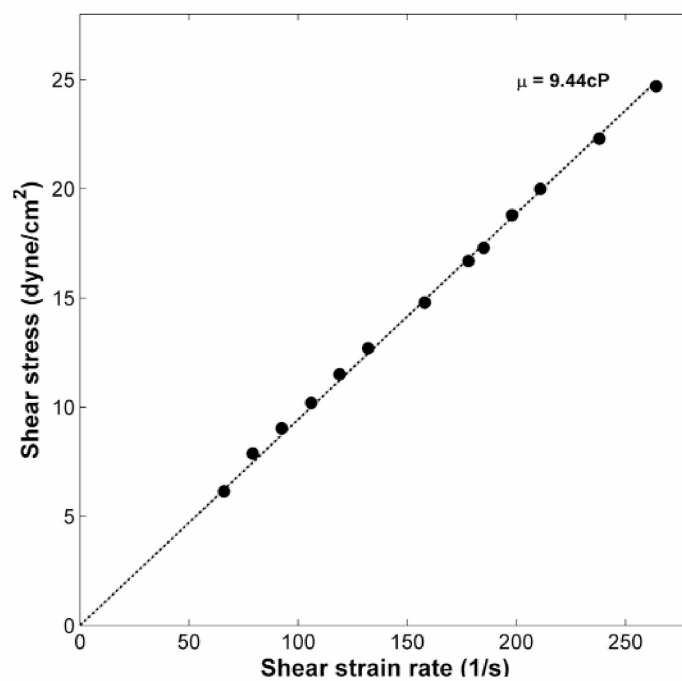


Figure 2.2 Calibration of the viscometer using standard newtonian calibration fluid provided by Brookfield at 25 °C.

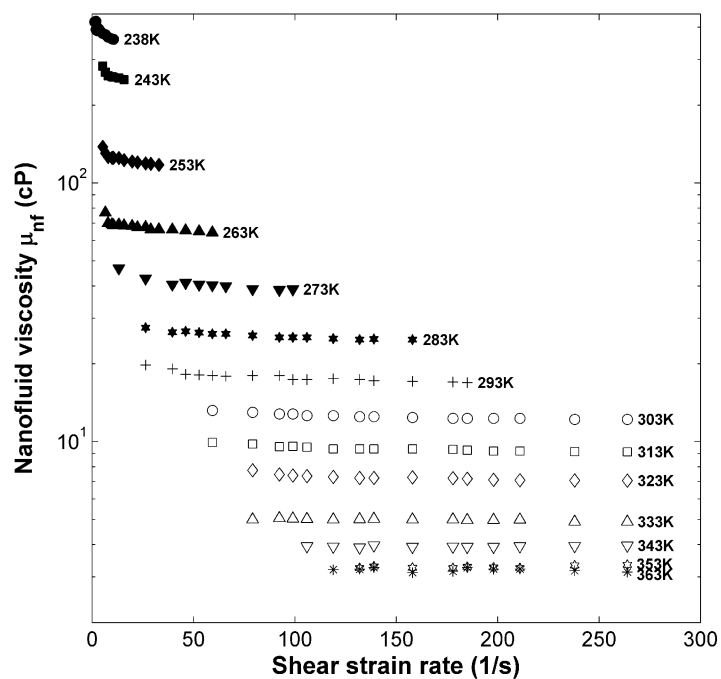


Figure 2.3 Viscosity variations with shear strain rate of  $\text{Al}_2\text{O}_3$  nanofluid of 10% concentration at various temperatures (238K to 363K).

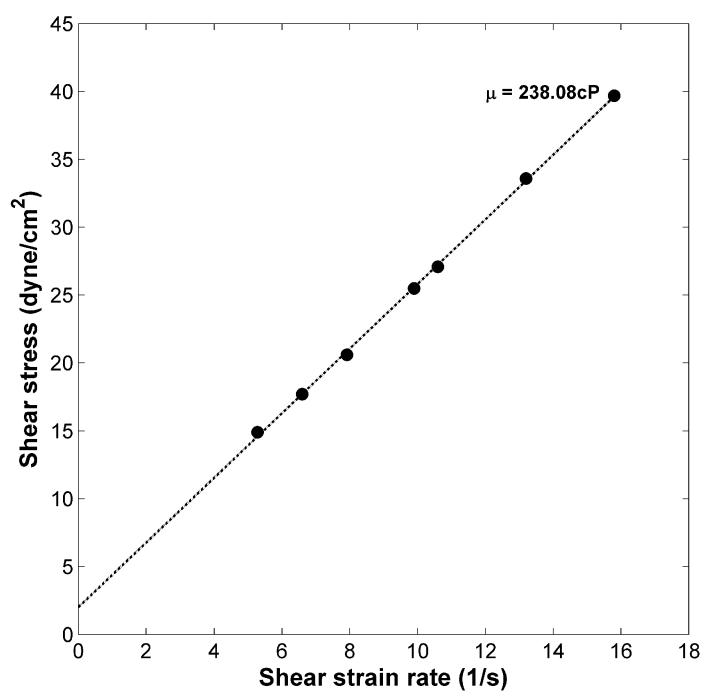


Figure 2.4 Nonnewtonian behavior of  $\text{Al}_2\text{O}_3$  nanofluid of 10% volumetric concentration at 243K.

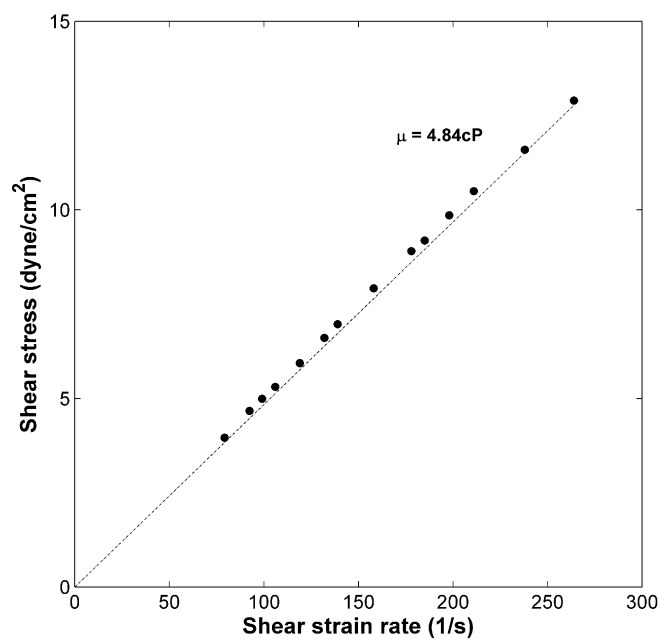


Figure 2.5 Shear stress versus shear strain rate for a 10% volume concentration of  $\text{Al}_2\text{O}_3$  nanofluid at 323K.

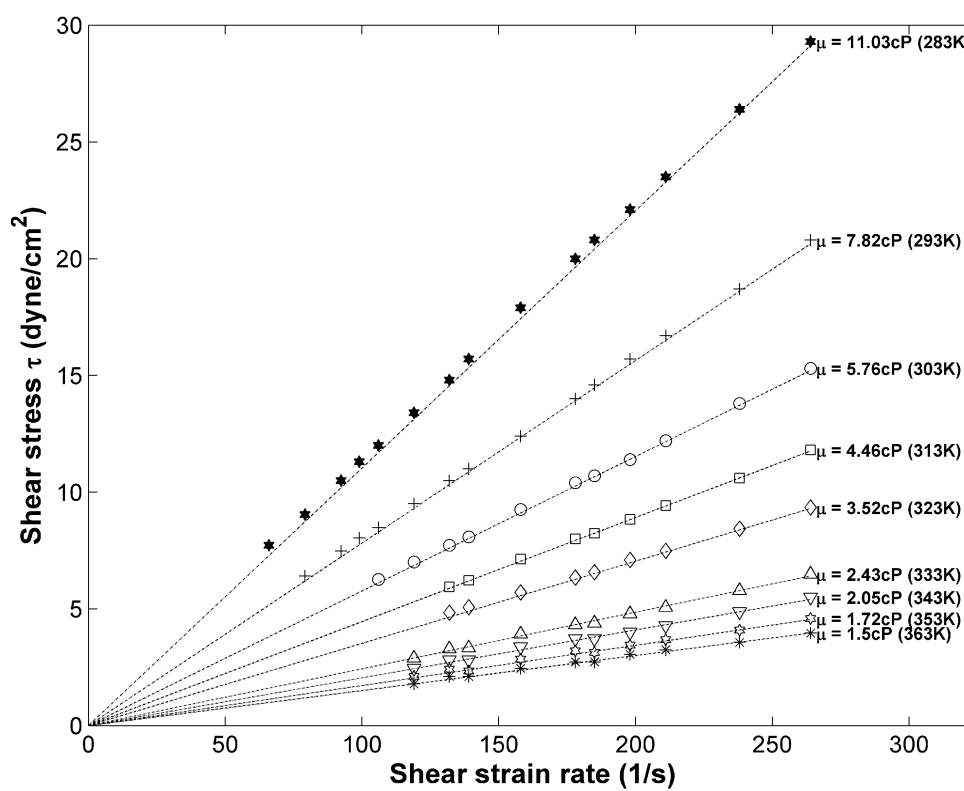


Figure 2.6 Shear stress versus shear strain rate in the higher temperature range (283K to 363K) for the 4%  $\text{Al}_2\text{O}_3$  nanofluid.

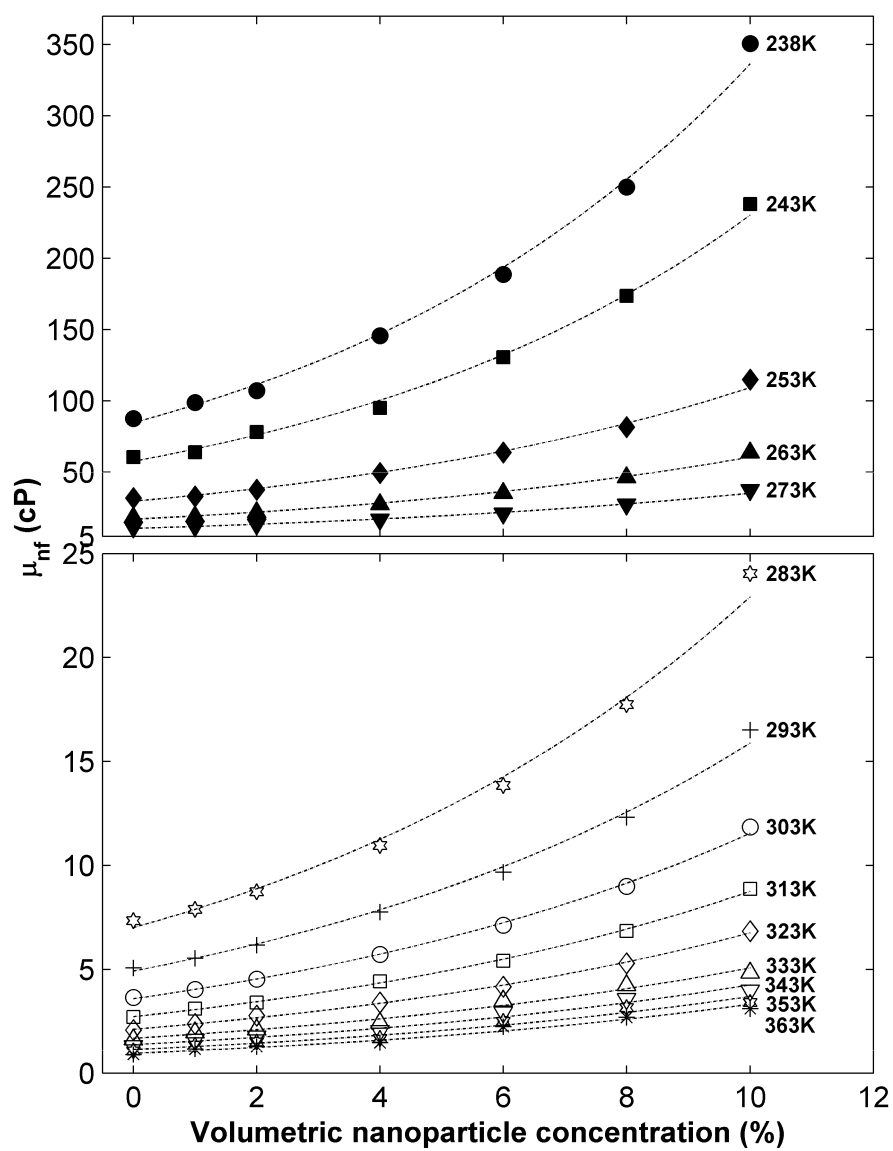


Figure 2.7 Variation of viscosity with volumetric concentrations at two distinct temperature regimes.

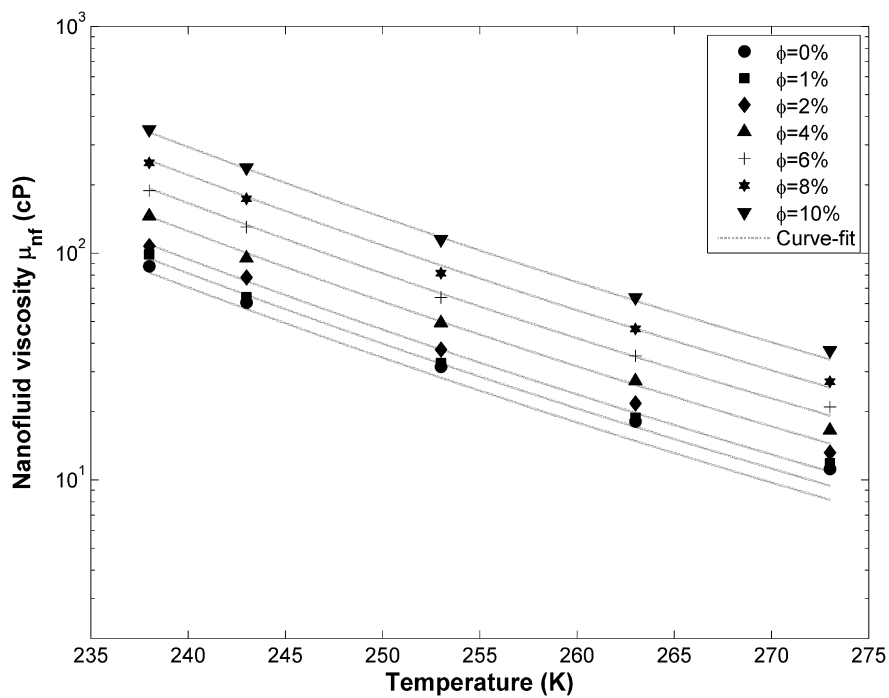


Figure 2.8 Experimental and curve-fit viscosity values for various concentrations of  $\text{Al}_2\text{O}_3$  nanofluid at low temperatures.

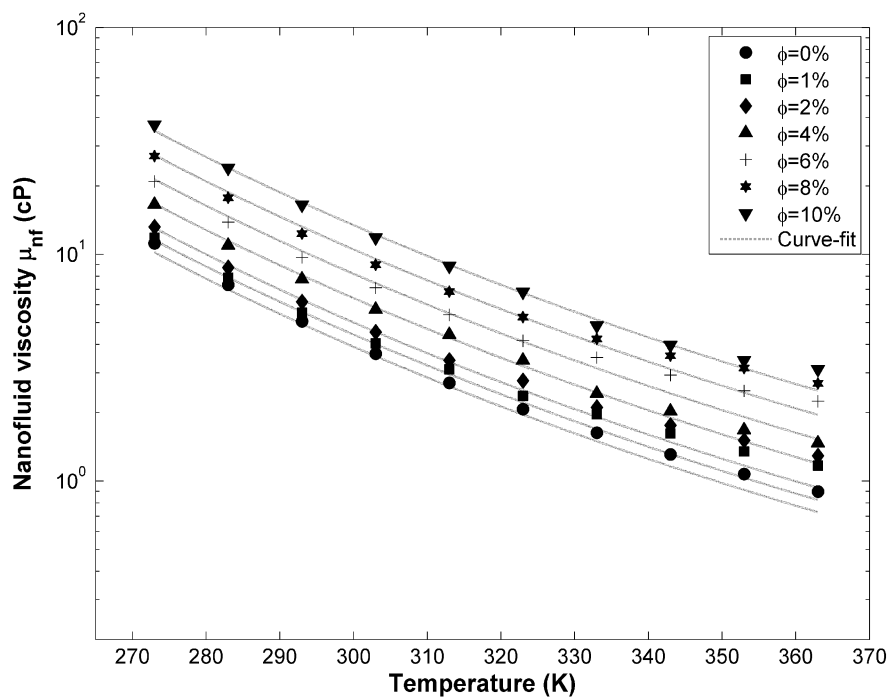


Figure 2.9 Experimental and curve-fit viscosity values for various concentrations of the  $\text{Al}_2\text{O}_3$  nanofluid at high temperatures.

## CHAPTER 3

### EXPERIMENTAL INVESTIGATION ON THE SPECIFIC HEAT OF ZINC OXIDE NANOFLUID<sup>1</sup>

#### Abstract

This paper describes a new apparatus and the procedure followed to measure the specific heat of nanofluids. A benchmark test case performed by measuring the specific heat of water by this apparatus shows that the accuracy of measurements is within  $\pm 1.5\%$  when compared to the data available in the literature. Following the benchmark test the apparatus was used to measure the specific heat of zinc oxide (ZnO) nanofluid prepared with a 60:40 ethylene glycol and water base fluid. The experimental results show that the specific heat decreases with an increase in particle volumetric concentration. However, it increases with an increase in temperature. A new correlation has been developed from the experimental data that expresses the specific heat of ZnO nanofluid as a function of temperature and concentration.

#### 3.1 Introduction

Advancements in nanotechnology have led to the development of nanofluids: nano-scale (less than 100nm particle size) metallic particles suspended in conventional heat transfer fluids such as water, ethylene or propylene glycol. Nanofluids have been shown to have greater convective heat transfer coefficients than fluids without the nanoparticles. This increase in heat transfer performance of nanofluids has spurred interest in developing nanofluids as a heat transfer medium. The laws of heat transfer dictate that a highly conductive fluid would greatly increase the efficiency of heat exchangers. These new fluids produce a need to develop devices to determine their thermal properties, one of which is the specific heat.

In Alaska and other cold regions, many residences and commercial buildings are heated using hydronic heating systems, where the working fluid is ethylene or propylene glycol and water mixture circulated at temperatures in the range of 310K to 363K. If nanofluids are proven successful, it will have a tremendous impact on the efficiency of heating systems by reducing the size of heat exchangers and the volume of fluid needed for heating applications. This lower

---

<sup>1</sup> Sahoo, B.C., P. Shymanski, D.K. Das and R. Ganguli. 2008. Experimental Investigation on the Specific Heat of Zinc Oxide Nanofluid. Published in Proceedings of the 40<sup>th</sup> Heat Transfer and Fluid Mechanics Institute, Sacramento, CA. pp 112-126

volume will result in less pumping power consumption and in turn will reduce the impact on the environment. In automobiles, nanofluid use will reduce radiator size. With nearly 400 million private vehicles in the United States, the impact in materials and energy savings will be enormous.

Very limited experimental data is currently available in the literature on the specific heat of nanofluids. Only Zhou and Ni [1] have reported specific heat measurements of water-based aluminum oxide nanofluid. The objective of this present research is to measure the specific heat of a nanofluid, viz. dispersion of ZnO nanoparticles of 77nm average particle size in a 60% ethylene glycol and 40% water mixture by mass (60:40 EG/W). Subsequently, the goal is to compare the available correlations with experimental data. Based upon this evaluation we develop a new correlation for the specific heat from the experimental data as a function of particle volumetric concentration  $\phi$  and temperature  $T$  of the nanofluid.

### 3.2 Theory

Specific heat of a nanofluid is the amount of heat required to increase the temperature of a unit mass by the fluid by one degree. There are two kinds of specific heats : specific heat at constant volume  $C_v$  and specific heat at constant pressure  $C_p$ . The constant-volume and constant-pressure specific heats are identical for nanofluids with a liquid as the base fluid, as the particles and the base fluid are both incompressible.

For nanofluids of mass  $m$  kg in a container, applying  $Q_1$  joules of heat to the fluid will raise its temperature by  $\Delta T$  Kelvin. The equation linking specific heat to these parameters are given by Cengel and Boles [2]

$$C_{pnf} = \frac{Q_1}{m(\Delta T)} \quad (1)$$

where  $C_{pnf}$  is the specific heat of the nanofluid in J/(kg.K).

The container should be well-insulated to minimize the heat loss to the surroundings. When a constant amount of electrical power  $\dot{Q}_{in}$  in watts is applied by an electric heating element to the nanofluid in a container for a period of time  $\Delta t$ , the heat budget of heating the container, heating element and insulation must be carefully determined to calculate  $Q_1$ , which is solely the heat absorbed by the nanofluid. From Eq. (1) knowing the heat input  $Q_1$  to the nanofluid, the mass

$m$  of the fluid and the change in temperature  $\Delta T$  over a period of time we can calculate the specific heat.

The final equation taking into account the heat absorbed by the container, heating element, insulation and the heat loss to the surroundings is given by the following equation.

$$C_{pnf} = \frac{(\dot{Q}_{in}\Delta t) - (m_c C_{pc}\Delta T_c) - (m_h C_{ph}\Delta T_h) - (m_i C_{pi}\Delta T_i) - (\dot{q}\Delta t)}{m_{nf}\Delta T_{nf}} \quad (2)$$

Under steady state condition the heat loss  $\dot{q} = k_{in}A \frac{(T_{in} - T_{on})}{L}$ .

where,

$\dot{Q}_{in}$  = Electrical power [W]

$\Delta t$  = Data acquisition time interval [s]

$m_c$  = Mass of container [kg]

$C_{pc}$  = Specific heat of container [J/(kg. K)]

$\Delta T_c$  = Change in temperature of container [K]

$m_h$  = Mass of heating element [kg]

$C_{ph}$  = Specific heat of heating element [J/(kg.K)]

$\Delta T_h$  = Change in temperature of heating element [K]

$\dot{q}$  = Heat loss through insulation [W]

$m_{nf}$  = Mass of nanofluid [kg]

$C_{pnf}$  = Specific heat of nanofluid [J/(kg.K)]

$\Delta T_{nf}$  = Change in temperature of nanofluid [K]

$m_i$  = Mass of insulation [kg]

$C_{pi}$  = Specific heat of insulation [J/(kg.K)]

$\Delta T_i$  = Change in temperature of insulation [K]

$T_{in}$  = Temperature on the inside of insulation [K]

$T_{on}$  = Temperature on the outside of insulation [K]

$A$  = Mean heat flow area through the insulation [m<sup>2</sup>]

$k_{in}$  = Thermal conductivity of the insulation [W/(m.K)]

$L$  = Thickness of the insulation [m]

For turbulent flow conditions, Dittus and Boelter [3] have proposed a correlation to determine the convective heat transfer in fluids

$$Nu = C Re^a Pr^b \quad (3)$$

where,

$Nu$  = Nusselt number =  $hd/k$

$h$  = Heat transfer coefficient of the fluid of thermal conductivity  $k$ , flowing in a tube of diameter  $d$

$Re$  = Reynolds number =  $Vd\rho/\mu$  :  $V$  is average velocity,  $\rho$  is the density and  $\mu$  is the dynamic viscosity of the fluid

$Pr$  = Prandtl number =  $C_p \mu / k$

The Prandtl number is a function of thermophysical properties and pivotal in the determination of convective heat transfer coefficients. Therefore, accurate determination of  $C_p$  is crucial to evaluate the heat transfer coefficient of nanofluids.

From experiments on  $\gamma\text{-Al}_2\text{O}_3$  and  $\text{TiO}_2$  nanofluids, Pak and Cho [4] proposed empirical values of the constants  $C=0.021$ ,  $a=0.8$  and  $b=0.5$ . Eq. (3) shows that the Nusselt number remains unchanged for different nanofluids with the same Reynolds number and Prandtl number. However, higher thermal conductivity of metallic nanoparticles than the base fluid increases the thermal conductivity of nanofluids. This results in a higher heat transfer coefficient, which provides enhanced heat transfer characteristics.

Moreover, the importance of accurate determination of  $C_p$  is evidenced by the fact that the total heat transfer rate  $\dot{q}$  through the wall of a heat exchanger flow passage (e.g. an automobile radiator or building heating coil) given by Eq. (4) (Bejan [5]), depends strongly on the former.

$$\dot{q} = \dot{m} C_p (T_i - T_o) \quad (4)$$

where  $\dot{m}$  = Mass flow rate,  $T_i$  = Inlet temperature and  $T_o$  = Outlet temperature

Another important parameter in heat transfer is the thermal diffusivity  $\alpha_{nf} = k_{nf} / (\rho_{nf} C_{pnf})$ , which is a function of specific heat [6]. In order to determine how fast heat will diffuse through the nanofluid this parameter must be known accurately. From the above discussions, it is apparent that accurate determination of  $C_p$  is very important in the evaluation of nanofluid thermal performance.

### 3.2.1 Specific Heat Correlations for Nanofluids

Pak and Cho [4] presented a simple mixture model for the specific heat of suspensions as a function of particle concentration and specific heat of each constituent.

$$C_{pnf} = (1 - \phi)C_{pbf} + \phi C_{ps} \quad (5)$$

where  $C_{pnf}$  = specific heat of nanofluid,  $C_{pbf}$  = specific heat of base fluid

$C_{ps}$  = specific heat of particle

$\phi$  = volumetric particle concentration

Buongiorno [7] included density in the above equation assuming that thermal equilibrium exists between the solid nanoparticles and the base fluid [Eq. (6)].

$$C_{pnf} = \frac{\phi \rho_s C_{ps} + (1 - \phi) \rho_{bf} C_{pbf}}{\rho_{nf}} \quad (6)$$

where  $\rho_s$  = density of solid nanoparticles,  $\rho_{bf}$  = density of base fluid and  $\rho_{nf}$  = density of nanofluid.

$$\rho_{nf} = \phi \rho_s + (1 - \phi) \rho_{bf} \quad (7)$$

Both Eq. (5) and (6) require determination of the specific heat of base fluid, which, in our case, is the 60:40 EG/W mixture. Specific heat data of the base fluid used in this research was obtained from ASHRAE [8]. Also, Eq. (6) requires determination of the base fluid density for computing the nanofluid specific heat. A correlation for the base fluid density was derived from the 60:40 mixture EG/W data provided by ASHRAE. A polynomial fit to the specific heat and density data yielded the correlations

$$C_{pbf} = 4.2483T + 1882.4 \quad 293\text{K} < T < 363\text{K}, \quad R^2 = 1 \quad (8)$$

$$\rho_{bf} = -0.00249T^2 + 0.9998T + 1002.5023 \quad 293\text{K} < T < 363\text{K}, \quad R^2 = 0.999 \quad (9)$$

where  $C_{pbf}$  in J/(kg.K) and  $\rho_{bf}$  = density in kg/m<sup>3</sup>.

The specific heat and density of the ZnO nanoparticles are taken to be 516.3 J/(kg.K) [9] and 5600 kg/m<sup>3</sup> (Alfa Aesar [10]), respectively.

### 3.3 Experimental Setup and Procedure

Figure 3.1 shows the experimental apparatus designed and constructed by Shymanski and Das [11] for measuring the specific heat of nanofluids. The nanofluid is placed in a rectangular

container (16.5 cm long  $\times$  14 cm wide  $\times$  5.1 cm deep), which is constructed from 0.63 cm thick chlorinated polyvinyl chloride (CPVC) material. This material is selected for its low cost and relatively low thermal conductivity, which minimizes the heat transmission through the CPVC wall, thus concentrating most of the heat within the nanofluid. There are two electrical heating coils of 100W capacity located symmetrically in the container for uniform distribution of heat. The nanofluid container is encased within 15.2 cm of styrofoam board insulation all around to minimize the heat loss from the container to the surroundings.

There are 10 copper-constantan thermocouples employed in this apparatus. Five thermocouples are submerged in the test fluid to obtain a mean temperature of the fluid. The thermocouples are distributed carefully at: center, side, rear, top and bottom of the container to ensure a minimum temperature gradient from thermocouple to thermocouple. One thermocouple is attached to the center of a heating coil. One thermocouple is used to record the temperature of the CPVC container. Four thermocouples are used to measure temperatures of the insulation at distances 0 cm, 5.1 cm, 10.2 cm and 15.3 cm; moving away from the container wall. Because the insulation is thick and a sizeable temperature gradient exists it is, it is divided to three layers (0-5.1, 5.1-10.2 and 10.2-15.3 cm) to accurately calculate the transient heating of each layer of the insulation.

A power meter is used to measure the input thermal power in watts entering the system. A variac connected to the power meter ensures a constant power supply. Two data loggers (Campbell Scientific 21X) collect temperature data from the test fluid, heating element, container and the insulation. Based upon tests with different rate of temperature rise a heat input of 35W was found to be the most suitable value for the apparatus. The dataloggers are programmed to record data at intervals of 15s. The mass of each component of the apparatus were recorded carefully by using a precision mass balance.

### **3.4 Results**

#### *3.4.1 Benchmark Test Case*

In order to ascertain the accuracy of the apparatus and the measurement procedure, a benchmark test case was performed to measure the specific heat of water, which is accurately known from the literature. A mass of 0.762 kg of water was taken as the sample fluid. It was subjected to a power input of 35W by the variac and monitored by the power meter. From this data the specific heat of water was calculated using Eq. (2). This experimental result is compared

in Figure 3.2 with the accurate values of  $C_p$  of water from Bejan [5]. Deviation of the experimental  $C_p$  from the values from Bejan is within  $\pm 1.5\%$ .

A plot of insulation temperatures versus time showed that the thermocouple attached on the outer surface of the insulation did not indicate any temperature rise. Therefore, the heat transmission did not reach the end of the insulation. As a result, there was no heat loss to the surroundings.

#### 3.4.2 ZnO Nanofluid Measurements

After verifying the apparatus and the procedure through the benchmark test case it was used to measure the specific heat of ZnO nanofluid. Four different volumetric concentrations (1, 3, 4 and 7%) of ZnO nanofluid were prepared by adding the correct amount of 50% ZnO nanoparticle suspension in water that was procured from the manufacturer, Alfa Aesar [10]. Using a precise mass balance the calculated amount of the base fluid (60:40 EG/W) was added to the concentrated solution to prepare the desired particle volumetric concentrations. The nanofluid was subjected to sonication for about an hour to ensure proper dispersion of nanoparticles before introducing it into the test container.

About 35W of power was applied for nearly two hours and temperatures were recorded by the thermocouples every 15s. From this data specific heat was computed using Eq. (2). The results of measured specific heat values are shown in Figure 3.3. We observe that the specific heat increases moderately with an increase in temperature and decreases with an increase in volumetric concentration.

Figure 3.4 shows the comparison of the measured specific heat with Pak and Cho [4] and Buongiorno [7] equations for the 7% concentration of ZnO nanofluid. An overprediction of about 30% by Pak and Cho equation is noticed. The error with Buongiorno equation increases with temperature reaching a value of about 7.5% at 360K. Therefore, it is imperative that a new correlation is needed for accurate prediction of specific heat.

#### 3.4.3 Development of the Specific Heat Correlation

Yaws [12] has recommended a cubic form of correlation in temperature for specific heat of many industrial chemicals. Das [13] developed such a cubic polynomial for aluminum oxide nanofluid, where the coefficients of the polynomial are functions of volumetric concentration. The same approach was applied here for the ZnO nanofluid. However, as Figure 3.5 shows the

data fits quite nicely for a first order polynomial for each concentration. Therefore, it is evident that the nanofluid specific heat is directly proportional to temperature  $T$  and inversely proportional to concentration  $\phi$ . Next, a single correlation was sought to combine the influence of temperature and concentration on specific heat.

Figure 3.6 shows the variation of  $C_{pnf}$  with concentration and temperature using the Labfit<sup>®</sup> software by Silva and Silva [14]. The resulting equation is

$$C_{pnf} = T/(A+B\phi) \quad (10)$$

The curve-fit parameters are:  $A = 0.1006$  and  $B = 3.688 \times 10^{-3}$ . In the above equation,  $0 < \phi \leq 7\%$  and  $310\text{K} < T < 363\text{K}$ . The deviation of the curve-fit values is within  $\pm 5\%$  of the experimental values.

### 3.5 Conclusions

A new apparatus has been constructed to measure the specific heat of nanofluids. It is an inexpensive device, but is accurate to within  $\pm 1.5\%$  in measuring the specific heat of water. Comparison of measured data with existing correlations showed that none of them predict specific heat accurately. From the experimental data a new correlation was developed for the specific heat of ZnO nanofluid. This correlation is much simpler than the existing correlations and predicts specific heat of ZnO nanofluid within  $\pm 5\%$  of the measured values. The apparatus is suitable for further measurements of different nanofluids to develop correlations similar to Eq. (10).

### References

- [1]. Zhou, S.Q. and Ni, R. (2008). Measurement of the specific heat capacity of water-based  $\text{Al}_2\text{O}_3$  nanofluid. *Applied Physics Letters*. 92(2): Art. No. 093123.
- [2]. Cengel, Yunus A. and Boles, Michael A. (2006). *Thermodynamics an Engineering Approach*. 5<sup>th</sup> Ed. McGraw Hill, New York.
- [3]. Dittus, P.W. and Boelter, L.M.K. (1930). *Heat transfer in automobile radiators of the tubular type*. In: Univ. California Pub. Eng. 2, No. 13, pp. 443-461; (1985) reprinted in *Intl. Comm. Heat Mass Transfer*. 12: pp. 3-22.
- [4]. Pak, B.C. and Cho, Y. I. (1998). Hydrodynamic and heat transfer study of dispersed fluids with submicron metallic oxide particles. *Experimental Heat Transfer*. 11: 151-170.
- [5]. Bejan, A (1993). *Heat Transfer*. John Wiley & sons, Inc., New York.

- [6]. White, F.M. (1988). *Heat and Mass Transfer*. Addison Wesley Publishing Co., New York.
- [7]. Buongiorno, J. (2006). Convective Transport in Nanofluids. *ASME Jour. of Heat Transfer*. vol. 128: pp. 240-250.
- [8]. ASHRAE. (2005). *ASHRAE Handbook – Fundamentals (SI)*. American Society of Heating, Refrigerating and Air-Conditioning Engineers Inc., Atlanta. 21.4-21.7.
- [9]. Adachi, S. (2004). *Handbook on Physical Properties of Semiconductors*. Springer-Verlag. Vol. 3: p68.
- [10]. Alfa Aesar. (2008). Available: <http://www.alfaesar.com>. Last accessed April 15, 2008.
- [11]. Shymanski, R.P. and Das, D.K. (2008). *Design, Construction and Testing of an Apparatus for Measuring the Specific Heat of Nanofluids*. Project Report submitted to EPSCOR Alaska, University of Alaska Fairbanks.
- [12]. Yaws, C.L. (1977). *Physical Properties – A Guide to the Physical, Thermodynamic and Transport Property Data of Industrially Important Chemical Compounds*. McGraw-Hill., New York.
- [13]. Das, D.K. (2008). Specific Heat Measurement of Different Nanofluids and Their influence on Heat Transfer. *Proceedings: Institution of Engineers (India), 49<sup>th</sup> Annual Technical Session*. Orissa State Center, India. 8 pp.
- [14]. Silva, Wilton P. and Silva, Cleide M.D.P.S. (2008). LAB Fit Curve Fitting Software (Nonlinear Regression and Treatment of Data Program) V 7.2.37 (1999-2007), Available: [www.labfit.net](http://www.labfit.net). Date of access: April 15, 2008.

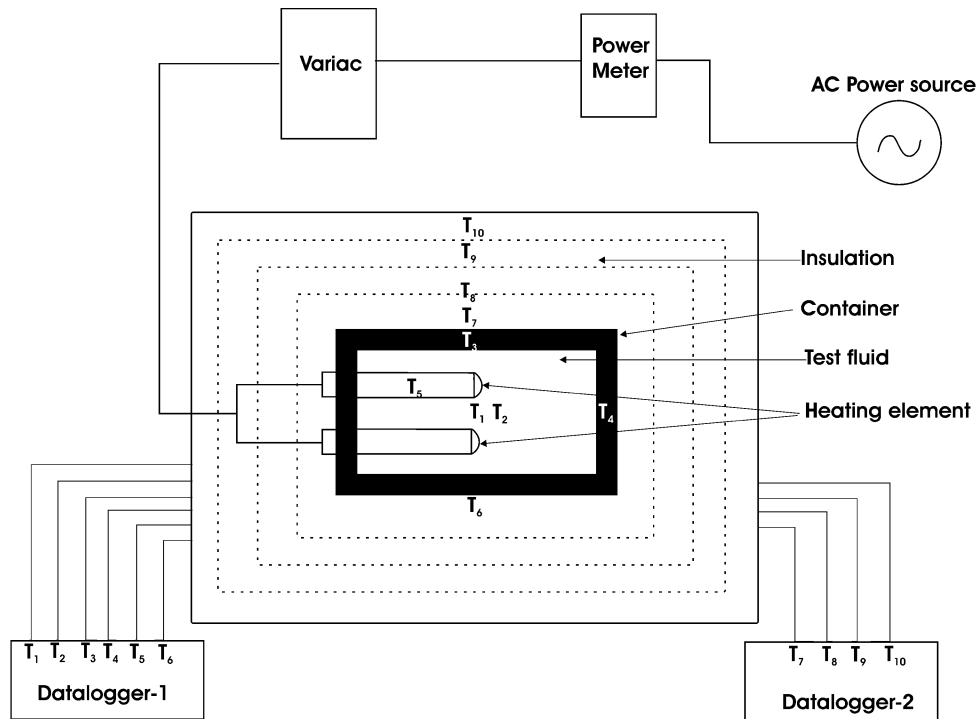


Figure 3.1 Experimental setup for the specific heat measurement.

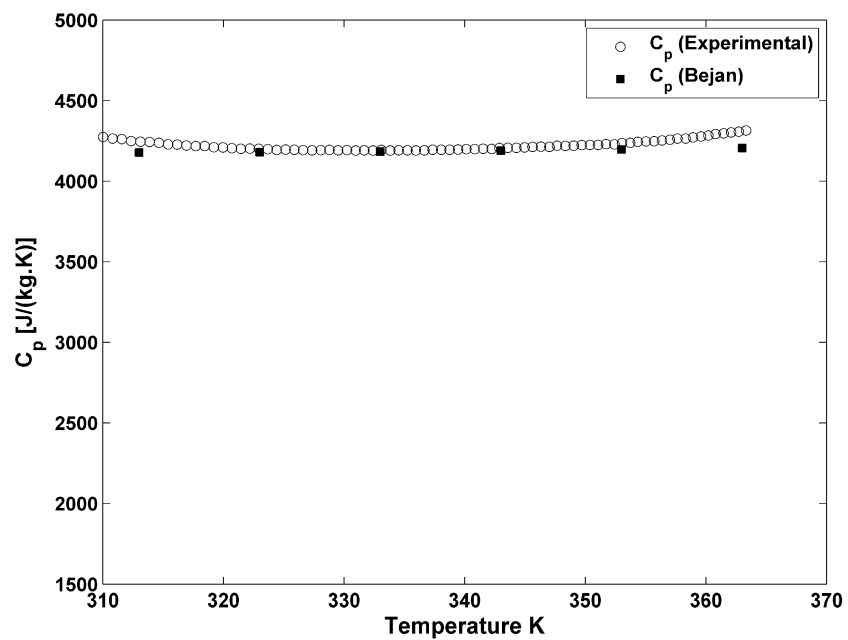


Figure 3.2 Comparison of measured specific heat of water with data from Bejan [5].

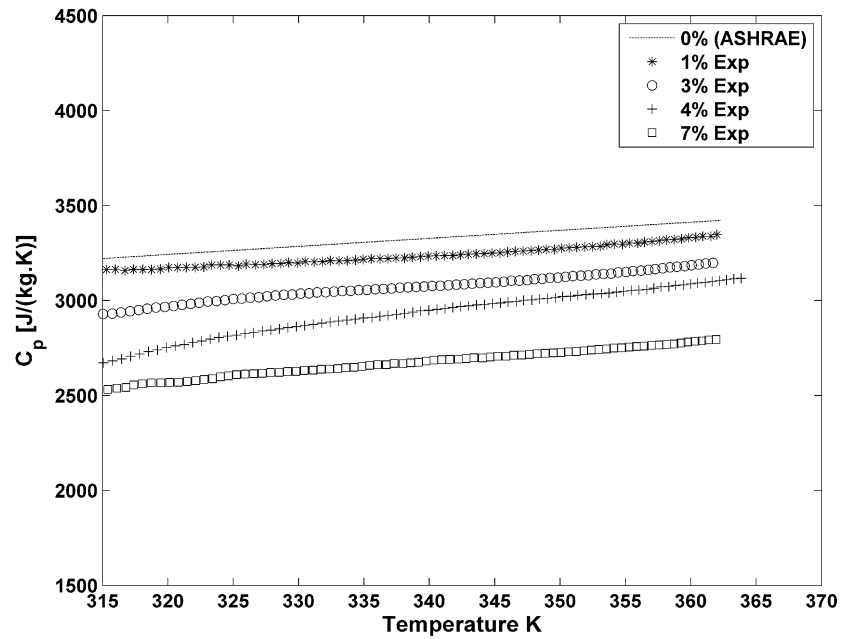


Figure 3.3 Measured specific heat of ZnO nanofluid as a function of temperature and concentration.

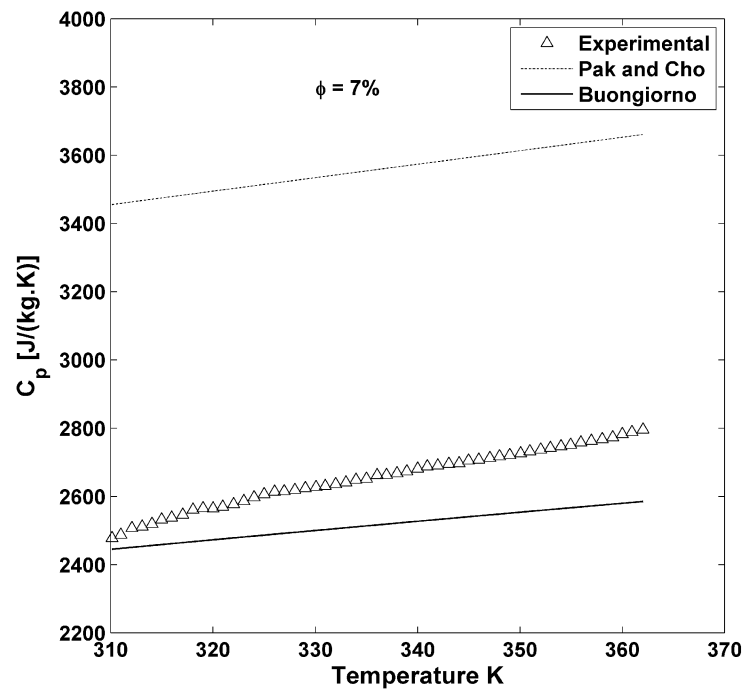


Figure 3.4 Comparison of experimental specific heat values with Pak and Cho [4] and Buongiorno [7] equations for ZnO nanofluid of 7% concentration.

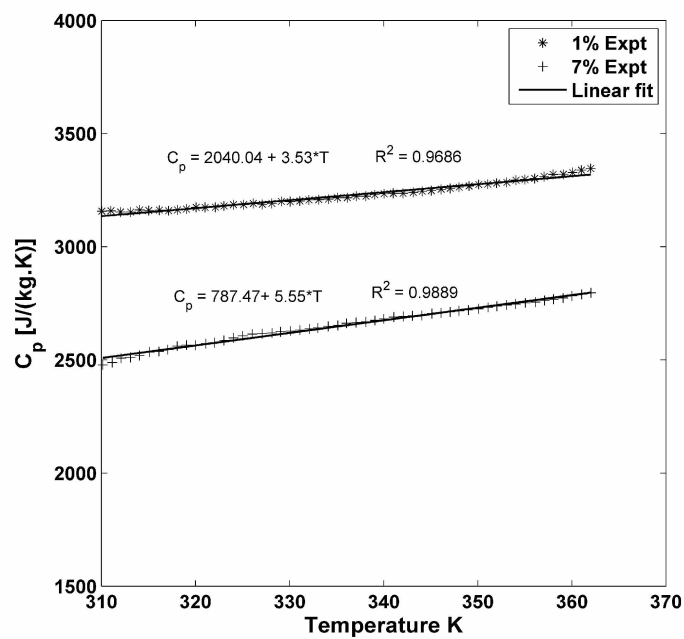


Figure 3.5 Variation of specific heat with temperature for 1% and 7% concentrations of ZnO nanofluid.

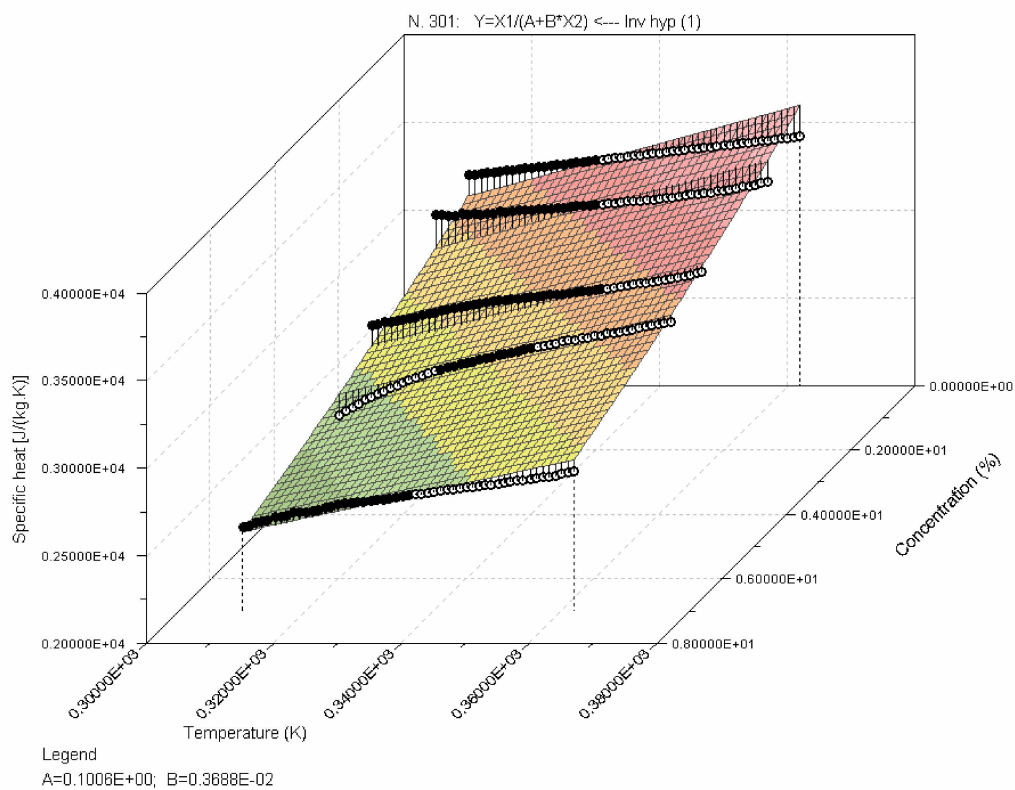


Figure 3.6 Specific heat as a function of temperature and concentration.

## CHAPTER 4

### NEW CORRELATIONS FOR THE THERMAL CONDUCTIVITY OF SILICON DIOXIDE NANOFLUID FROM EXPERIMENTS<sup>1</sup>

#### Abstract

Experimental investigations have been carried out for the determination of thermal conductivity of silicon dioxide nanoparticles dispersed in 60% ethylene glycol and 40% water by mass. Experiments conducted in a temperature range of 298 K to 365 K and for particle volumetric concentrations up to 10% show that the ratio of thermal conductivity of nanofluid to that of the base fluid increases with an increase in temperature and concentration. Comparisons of experimental results of this non-metallic nanoparticle suspension with some existing models proposed for metallic nanofluids do not exhibit good agreement. Therefore, an existing model was modified by incorporating new correlations derived from the experimental data. In this model, thermal conductivity is expressed as a function of temperature, concentration and the properties of the base fluid and nanoparticles.

**Keywords:** nanofluids, silicon dioxide, thermal conductivity, non-metallic, temperature dependency, concentration

#### Nomenclature

$C_p$	Specific heat [J/(kg.K)]
$d_p$	Particle diameter [m]
$k$	Thermal conductivity [W/(m.K)]
$T$	Temperature [K]
Greek Letters	
$\phi$	Particle volumetric concentration
$\rho$	Density of the fluid [kg/m <sup>3</sup> ]
$\kappa$	Boltzmann constant = $1.381 \times 10^{-23}$ J/K

---

<sup>1</sup> Sahoo, B.C., D.K. Das and R. Ganguli. 2008. New Correlations for the Thermal Conductivity of Silicon Dioxide Nanofluid from Experiments. Submitted for publication to Micro and Nano Letters.

### Subscripts

<i>bf</i>	Base fluid
<i>nf</i>	Nanofluid
<i>p</i>	Particle

## 4.1 Introduction

Nanofluids are suspensions of nanometer-size particles (<100 nm) suspended in base fluids such as water, ethylene glycol and oil. With the increasing energy demand of modern society, nanofluid research has received great attention due to the enhanced thermal characteristics of nanofluids. For example, Eastman et al. [1] have shown that effective thermal conductivity of ethylene glycol is increased by about 40% when copper nanoparticles of average particle size 10 nm and 0.3% volumetric concentration are dispersed in it. Since for a given Nusselt number, the convective heat transfer coefficient of a fluid is directly proportional to its thermal conductivity, its accurate determination is very important in evaluating the thermal performance of nanofluids.

Lee et al. [2] reported over 20% thermal conductivity enhancement of ethylene glycol when CuO particles of 4% volumetric concentration were suspended in it. Thermal conductivity of low concentration (up to 4%) aqueous suspensions of Al<sub>2</sub>O<sub>3</sub> and CuO in a temperature range of 21°C to 51°C was measured by Das et al. [3]. They observed that for 1% CuO-water nanofluid, the thermal conductivity ratio of nanofluid to that of base fluid increased from 6.5% to 29% over a temperature range of their experiments.

Based on the concept of a nanolayer around smaller nanoparticles, Yu and Choi [4] proposed a modified version of the model suggested by Maxwell [5]. Effect of Brownian movements of nanoparticles on thermal conductivity was considered in a model proposed by Koo and Kleinstreuer ([6], [7]) combining a static and a dynamic term, which showed good agreement for several nanofluids. Experimental results on thermal conductivity of a 5% TiO<sub>2</sub>-water nanofluid by Murshed et al. [8] deviated by about 17% from the widely used Hamilton-Crosser [9] and Bruggemen [10] models. Another thermal conductivity model was proposed by Prasher et al. [11], which was a combination of the Brownian Reynolds number and a Maxwell-Garnet composite model. The model developed by Jang and Choi [12] considered collisions among the

base fluid molecules and nanoparticles; thermal diffusion of nanoparticles in the base fluid and nano-convection due to Brownian motion. Comparison of transient and steady-state thermal conductivity of Al<sub>2</sub>O<sub>3</sub>-water nanofluids up to a concentration of 6% by Li et al. [13] showed that while at room temperature both the methods showed very little variation, at higher temperatures the transient method yielded higher thermal conductivity values due to natural convection. For a comprehensive review of both theoretical and experimental studies on nanofluid thermal conductivity, the reader may refer to Wang and Mujumdar [14].

Thermal conductivity data and models discussed in the above sections consider metallic nanoparticles in either water or glycol-based fluids. However, research in the area of non-metallic nanofluids (e.g. SiO<sub>2</sub>) is very limited. Especially, no data is available on SiO<sub>2</sub> nanofluids in a 60:40 EG/W base fluid, although it is the most commonly used heat transfer fluid in cold regions. From an economical view point, SiO<sub>2</sub> nanofluid may be a viable fluid because it is presently the least expensive nanofluid available commercially. Therefore, in the present research, thermal conductivity of 60:40 EG/W based SiO<sub>2</sub> nanofluid in a temperature range of 298K to 363K and particle concentrations up to 10%, are experimentally determined. This temperature range is the operational range of building heating fluids, automobile coolants and industrial heat exchangers in cold regions. From the experimental data, temperature and concentration dependency of thermal conductivity is studied. The model of Koo and Kleinstreuer ([6], [7]) was modified with two new correlations for the SiO<sub>2</sub> nanofluid.

The nanofluid used in this study was procured from Alfa Aesar [15] as a 50% (by mass) aqueous suspension with average nanoparticle size of 30 nm. The manufacturer supplied nanofluid was diluted by addition of deionized water. Uniform dispersion of nanoparticles in the suspension was ensured by ultrasonication of the test fluids for about 2 hours prior to the experiments.

#### 4.2 Existing Thermal Conductivity Models

Pioneer work in thermal conductivity modeling of suspensions was done by Maxwell [5], which holds for spherical micro- and milli-meter size particles of low concentrations :

$$k_{eff} = \frac{k_p + 2k_{bf} + 2(k_p - k_{bf})\phi}{k_p + 2k_{bf} - (k_p - k_{bf})\phi} k_{bf} \quad (1)$$

where,  $k_{eff}$  is the effective thermal conductivity;  $k_{bf}$  and  $k_p$  are the thermal conductivities of the base fluid and suspended particles, respectively.  $\phi$  is the particle concentration.

Bruggemen [10] proposed a model for spherical particles for any concentration. Hamilton and Crosser [9] included an empirical shape factor ( $n$ ) for the suspended particles in their model with  $n = 3$  for perfectly spherical particles.

$$k_{eff} = \frac{k_p + (n-1)k_{bf} - (n-1)\phi(k_{bf} - k_p)}{k_p + (n-1)k_{bf} + \phi(k_{bf} - k_p)} k_{bf} \quad (2)$$

All the above models were developed for particle size in micro- or greater ranges and are not suitable to model nanofluid thermal conductivity. Therefore, several theoretical and experimental models have been developed in recent years to predict thermal conductivity of nanofluids. In most of the models Brownian motion of nanoparticles is accounted for (e.g. [6], [7], [11], [12] and [16]) to predict thermal conductivity. The model developed by Koo and Kleinstreuer ([6], [7]) improved the Brownian effect by introducing two correlations. Their model is:

$$k_{nf} = \frac{k_p + 2k_{bf} - 2(k_{bf} - k_p)\phi}{k_p + 2k_{bf} + (k_{bf} - k_p)\phi} k_{bf} + 5 \times 10^4 \beta \phi \rho_{bf} C_{pbf} \sqrt{\frac{\kappa T}{\rho_p d_p}} f(T, \phi) \quad (3a)$$

where  $\beta$  represents the fraction of the liquid volume which travels with a particle. The function  $\beta$  obtained by them for different nanoparticles as a function of particle volume concentrations are:

$$\text{CuO} : 0.0011(100\phi)^{-0.7272} \quad \text{and} \quad \text{Al}_2\text{O}_3 : 0.0017(100\phi)^{-0.0841} \quad \phi > 1\% \quad (3b)$$

Since from the kinetic theory, the dependence of thermal conductivity on temperature is weak, they introduced an empirical function  $f(T, \phi)$  using the experimental data of Das et al. [3] on CuO nanofluids.

$$f(T, \phi) = (-6.04\phi + 0.4705)T + (1722.3\phi - 134.63) \quad (3c)$$

They recommended the above equation in the ranges  $1\% < \phi < 4\%$  and  $300 \text{ K} < T < 325 \text{ K}$ . The first part of the Eq. (3a) is the particles' conventional static conductivity obtained directly from the Maxwell model while the second part accounts for the Brownian motion.

#### 4.3 Experimental Setup and Procedure

A heat transfer service unit (Model H111) with the apparatus for thermal conductivity of liquids and gases manufactured by P.A. Hilton Ltd. [17] was used for the experiments (Figure 4.1). The fluid whose thermal conductivity is to be measured is slowly injected into the annular

spacing to prevent inclusion of air bubbles. The annular spacing  $\Delta r$  between the water-cooled jacket and the cylindrical plug encasing a cartridge heater is made very small ( $= 0.3$  mm) in order to prevent natural convection. The aluminum plug has low thermal inertia and minimal temperature variation along its length. The plug is held in a central position inside the cylinder by ‘O’ rings that seal the annular spacing. Precision thermocouples placed on the external surface of the plug and the internal surface of the cooling jacket effectively measure temperatures of the hot and cold faces of the fluid lamina, respectively. Temperatures are recorded by both the heat transfer service unit and a data logger for error-checking and comparison. Total electric power input  $\dot{Q}_e$  to the heater, and hence the aluminum plug, is measured by the voltmeter and ammeter housed inside the service unit.

The conduction heat transfer rate  $\dot{Q}_c$  through the fluid lamina is the difference between  $\dot{Q}_e$  and the incidental heat transfer rate  $\dot{Q}_i$ . This  $\dot{Q}_i$  is the sum of heat losses from the heater other than that transferred by conduction through the fluid and is obtained from a calibration curve. Air is used as the test fluid to develop the calibration curve for this apparatus as per the recommendation of the manufacturer, because its thermal conductivity is known accurately. Details of the apparatus calibration are discussed in Section 3.1. The input power is gradually increased by increasing the voltage and current in steps via the panel mounted control knob. Temperatures  $T_1$  and  $T_2$  are measured when thermal equilibrium is reached. Thus, this apparatus provides a steady state method for determining the thermal conductivity of fluids and differs from the transient hot wire method.

Finally, thermal conductivity of the nanofluid  $k_{nf}$  is given as

$$k_{nf} = \frac{\dot{Q}_c \Delta r}{A(\Delta T)} \quad (4)$$

where  $A$  is the effective area of conducting path through the fluid provided by the manufacturer.

#### 4.3.1 Development of Calibration Curve

Incidental heat transfer  $\dot{Q}_i$  includes heat (i) conducted from the plug to the jacket by the ‘O’ ring seals, (ii) radiated from the plug to the jacket and (iii) losses to the surroundings from the exposed ends of the plug. Since manufacturing specifications may differ from one unit to another, the manufacturer recommends calibration of the apparatus using air as the test fluid.

Annular spacing  $\Delta r$  between the plug and the jacket was filled with air and both ends of the flexible tubes (marked “fluid injection” and “vent” in Figure 4.1) are closed tightly. Transformer voltage was adjusted to 50V and when stabilized, the plug  $T_1$  and jacket  $T_2$  surface temperatures were recorded along with voltage  $V$  and current  $I$ . This process was repeated for voltages up to 244V with approximately uniform temperature differences. Mean air temperature  $T_m = (T_1+T_2)/2$ , temperature difference  $\Delta T = (T_1-T_2)$ , electrical power input  $\dot{Q}_e = V \times I$  and heat conducted through air  $\dot{Q}_c = (k_{air} A \Delta T) / \Delta r$  are computed. Thermal conductivity of air  $k_{air}$  at temperature  $T_m$  is obtained from Incropera and DeWitt [18]. Mean surface area  $A$  (0.0133 m<sup>2</sup>) and annular spacing  $\Delta r$  are taken from the manufacturer specifications. Incidental heat transfer  $\dot{Q}_i = \dot{Q}_e - \dot{Q}_c$  is tabulated against the temperature differences  $\Delta T$  and plotted as the calibration curve (Figure 4.2). From this plot the equation for incidental heat transfer is

$$\dot{Q}_i = 0.2097 (\Delta T) \text{ with } R^2 = 0.9989 \text{ and } 0 \text{ K} < \Delta T < 65 \text{ K} \quad (5)$$

#### 4.3.2 Uncertainty in Thermal Conductivity Measurements

The uncertainty associated with thermal conductivity measurements was estimated using the standard approach proposed by Coleman and Steele [19]. The quantities involved in thermal conductivity measurements are :  $\dot{Q}_e$ ,  $\dot{Q}_i$ ,  $\Delta r$ ,  $A$  and  $\Delta T$ , as defined earlier in this paper. Therefore, the uncertainty in measuring  $k$  can be written as

$$\frac{\delta k}{k} = \left[ \left( \frac{\delta \dot{Q}_e}{\dot{Q}_e} \right)^2 + \left( \frac{\delta \dot{Q}_i}{\dot{Q}_i} \right)^2 + \left( \frac{\delta(\Delta r)}{\Delta r} \right)^2 + \left( \frac{\delta A}{A} \right)^2 + \left( \frac{\delta(\Delta T)}{\Delta T} \right)^2 \right]^{1/2} \quad (5a)$$

The uncertainty in measuring voltage ( $\delta V/V$ ) and current ( $\delta I/I$ ) are about 0.5%. Therefore, the uncertainty in measuring  $\dot{Q}_e = VI$  is

$$\frac{\delta \dot{Q}_e}{\dot{Q}_e} = \left[ \left( \frac{\delta V}{V} \right)^2 + \left( \frac{\delta I}{I} \right)^2 \right]^{1/2} \quad (5b)$$

Uncertainties associated with  $\dot{Q}_i$  is due to the  $\Delta T$  measurement

$$\frac{\delta \dot{Q}_i}{\dot{Q}_i} = \left[ \left( \frac{\delta T_1}{T_1} \right)^2 + \left( \frac{\delta T_2}{T_2} \right)^2 \right]^{1/2} \quad (5c)$$

The uncertainty of temperature measurements for type-K thermocouples [20] used in this apparatus is 0.6 °C in a range of 273 K to 373 K. For the range of temperatures considered in this research the uncertainty attributed to thermocouples ( $\delta T/T$ ) can be estimated at mean temperature of 323 K and is found to be 1%. The uncertainty in length measurement  $\delta r/r$  by the modern metrological gauge is about 0.5 %. Consequently, uncertainty in area measurement is :  $\delta A/A = \left[ (2\delta L/L)^2 \right]^{1/2}$ , where  $L$  is a length dimension. The uncertainty in measuring  $\Delta T$  is

$$\frac{\delta(\Delta T)}{\Delta T} = \left[ \left( \frac{\delta T_1}{T_1} \right)^2 + \left( \frac{\delta T_2}{T_2} \right)^2 \right]^{1/2} \quad (5d)$$

Combining all the above uncertainties, the uncertainty in measurement of  $k$  is given as :

$$\begin{aligned} \frac{\delta k}{k} &= \left[ \left( \frac{\delta V}{V} \right)^2 + \left( \frac{\delta I}{I} \right)^2 + \left( \frac{\delta T_1}{T_1} \right)^2 + \left( \frac{\delta T_2}{T_2} \right)^2 + \left( \frac{\delta r_1}{r_1} \right)^2 + \left( \frac{\delta r_2}{r_2} \right)^2 + \left( 2 \frac{\delta L}{L} \right)^2 + \left( \frac{\delta T_1}{T_1} \right)^2 + \left( \frac{\delta T_2}{T_2} \right)^2 \right]^{1/2} \\ &= 2.45\% \end{aligned} \quad (5e)$$

## 4.4 Results and Discussion

### 4.4.1 Benchmark Test Case

A benchmark test case was performed with 60:40 EG/W mixture prior to the thermal conductivity experiments to establish the correctness of the apparatus and procedure. Accurate thermal conductivity values of this mixture in the experimental temperature range are obtained from the American Society of Heating, Refrigeration and Air-conditioning Engineers (ASHRAE) [21] and compared with the values obtained from experiments (Figure 4.3). The maximum deviation between the measured values and ASHRAE data is only 0.4% at 343 K, verifying the accuracy of the apparatus and the experimental procedure. The benchmark test fluid is also the base fluid used in this research and the correlation between temperature and thermal conductivity as shown in Figure 4.3, is used in subsequent sections to calculate thermal conductivity of base fluid ( $k_{bf}$ ) at any given temperature. For the thermal conductivity of the base fluid a second order polynomial in temperature was derived by curve-fitting the ASHRAE data.

$$k_{bf} = -3.4216 \times 10^{-6} T^2 + 0.00266 T - 0.13068 \quad \text{with } R^2 = 0.9971 \quad 290 \text{ K} < T < 365 \text{ K} \quad (6)$$

#### 4.4.2 Thermal Conductivity of SiO<sub>2</sub> Nanofluid

After qualifying the apparatus and experimental procedure through the benchmark test case, thermal conductivity of SiO<sub>2</sub> nanofluid of different volumetric concentrations in a base fluid of 60:40 EG/W was measured and the results plotted in Figure 4.4. It is observed that within the experimental temperature range the thermal conductivity of each concentration increases as a quadratic function of the fluid temperature. As an example, the thermal conductivity of a 6% concentration of nanofluid can be represented by

$$k_{\text{nf}} = -1.897 \times 10^{-6} T^2 + 0.0021 T - 0.06618 \quad \text{with } R^2 = .9987 \quad 298 \text{ K} < T < 365 \text{ K} \quad (7)$$

This observation is similar to what was noticed for the base fluid in Eq. (6). Also, thermal conductivity increases with particle concentration, since the higher thermal conductivity particles were added to a fluid of lower thermal conductivity. A comparison of the experimental thermal conductivity with the values predicted by Hamilton-Crosser [9] correlation presented as Eq. (2) for two concentrations (viz. 1% and 6%) of SiO<sub>2</sub> nanofluid is shown in Figure 4.4. It is observed that the Hamilton-Crosser correlation underpredicts the nanofluid thermal conductivity. For the Hamilton-Crosser correlation, although thermal conductivity increases with concentration, the temperature influence is less dominant. We observe larger deviations of the predicted thermal conductivity from the experimental values at higher temperatures. Thus, the Hamilton-Crosser model fails to predict thermal conductivity of the SiO<sub>2</sub> nanofluid.

It is always desirable to examine the non-dimensional thermal conductivity ratio  $k_r$  of the nanofluid, when it is normalized by the base fluid value, because the thermal behavior will also include the influence of the base fluid. This ratio, called the relative thermal conductivity is plotted against temperature in Figure 4.5. An increase in thermal conductivity of the base fluid due to the addition of nanoparticles is observed. An enhancement of the relative thermal conductivity with an increase in temperature as well as the volumetric concentration is noticed. For a 10% concentration  $k_r$  increases by 7% and 11% at 300 K and 365 K, respectively, over the base fluid. For the same concentration,  $k_r$  increases from 1.065 to 1.105, a 3.6% increase between 298 K and 365 K. Therefore, the application of nanofluids at higher temperatures will yield a better dividend.

Relationship between relative thermal conductivity and particle volumetric concentration of SiO<sub>2</sub> nanofluid is shown in Figure 4.6. Relative thermal conductivity values calculated at four different temperatures (298 K, 313 K, 333 K and 363 K) using both the Hamilton-Crosser and experimental correlations are shown in this figure. It is observed that thermal conductivity

increases with an increase in concentration at various temperatures. The correlation between  $\phi$  and  $k_r$  at a given temperature, shown by solid lines appears to be a quadratic function of  $\phi$ . For example, for a temperature of 333 K the thermal conductivity ratio  $k_r$  can be expressed as

$$k_r = 2.0246\phi^2 + 0.5043\phi + 1.0955 \quad \text{with } R^2 = 0.9957 \quad 0.01 \leq \phi \leq 0.10 \quad (8)$$

It is clear that Hamilton-Crosser correlation does not match the experimental data. Therefore, a new correlation is warranted to correctly predict the thermal conductivity of SiO<sub>2</sub> nanofluids.

#### 4.5 Development of New Correlation

For the SiO<sub>2</sub> nanofluid, 46 measurements spanning a temperature range of 298 K to 365 K and particle concentrations of 1 to 10% were experimentally obtained. On comparison of the experimental values with several existing correlations it was found that the Koo and Kleinstreuer [6] model matched the experimental results more closely than any other correlation. Nevertheless, the Koo and Kleinstreuer correlation was developed for a limited temperature range (293 K to 325 K) and concentration below 4% for metallic nanoparticles. Therefore, we propose a new correlation for the SiO<sub>2</sub> nanofluid based on the experimental data collected over wider temperature and concentration ranges. From this experimental data, modified empirical correlations for  $\beta$  and  $f(T, \phi)$  were derived for the Koo and Kleinstreuer model.

$$k_{nf} = \frac{k_p + 2k_{bf} - 2(k_{bf} - k_p)\phi}{k_p + 2k_{bf} + (k_{bf} - k_p)\phi} k_{bf} + 5 \times 10^4 \beta \phi \rho_{bf} C_{pbf} \sqrt{\frac{\kappa T}{\rho_p d_p}} f(T, \phi) \quad (9a)$$

$$\beta = 1.9526 (100\phi)^{-1.4594} \quad (9b)$$

$$f(T, \phi) = (1.0336 \times 10^{-4} \phi + 1.4348 \times 10^{-5}) T + (-3.0669 \times 10^{-2} \phi - 3.91123 \times 10^{-3}) \quad (9c)$$

for  $1\% \leq \phi \leq 10\%$  and  $298 \text{ K} < T < 365 \text{ K}$ . For the new model  $\rho_{bf}$  and  $C_{pbf}$  are obtained from the ASHRAE data and  $k_p = 1.38 \text{ W/(m.K)}$  and  $\rho_p = 2220 \text{ kg/m}^3$  are taken from Incropera and DeWitt [18].

The new model was verified by calculating the thermal conductivity of SiO<sub>2</sub> nanofluids using Eq.s 9(a)-(c). It is found that the experimental values exhibit good agreement with the model results shown in Figure 4.7. A maximum overprediction of 3.35% and underprediction of 1.95% between the model and the measured thermal conductivity are observed. The average deviation is 1.16% and the root mean square deviation is 0.79%. Therefore, this model can be

used for accurate prediction of the thermal conductivity of SiO<sub>2</sub> nanofluids for the specified range of temperature and concentration.

#### 4.6 Conclusions

A set of thermal conductivity values for the non-metallic SiO<sub>2</sub> nanofluid were obtained from careful experimental observations over a broad temperature range of 298 K to 365 K and particle volumetric concentrations ranging from 1% to 10% in a 60:40 EG/W base fluid. Thermal conductivity increased with both temperature and concentration. Existing thermal conductivity models for suspensions fail to predict thermal conductivity of SiO<sub>2</sub> nanofluids. The Hamilton-Crosser model do not account for the effect of temperature and concentration on thermal conductivity enhancement properly. A set of new correlations were proposed by improving the Koo and Kleinstreuer [6] model using the experimental data collected over a broader range of temperature and concentrations. These new correlations predict thermal conductivity of SiO<sub>2</sub> nanofluids with a maximum deviation of 3.35% from the experimental values. Also, it is observed that nanofluids exhibit superior thermal conductivity at higher temperatures and hence their application at high temperatures may be more preferable.

#### Acknowledgements

Partial financial assistance for this research was provided to the first author by the Office of Electronic Miniaturization at the University of Alaska Fairbanks through a DARPA grant.

#### References

- [1] Eastman, J.A., Choi, S.U.S, Li, S., Yu, W. and Thompson, L.J. (2001). Anomalously increased effective thermal conductivities of ethylene glycol-based nanofluids containing copper nanoparticles. *Applied Physics Letters*. 78 (6): 718-720.
- [2] Lee, S., Choi, S.U.S., Li, S. and Eastman, J. (1999). Measuring thermal conductivity of fluids containing oxide nanoparticles. *Jour. Heat Transfer*. 121: 280-289.
- [3] Das, S., Putra, N., Thiesen, P. and Roetzel, W. (2003). Temperature dependence of thermal conductivity enhancement for nanofluids. *Jour. Heat Transfer*. 125: 567-574.
- [4] Yu, W. and Choi, S. (2003). The role of interfacial layers in the enhanced thermal conductivity of nanofluids: A renovated Maxwell model. *Jour. Nanoparticle Res.* 5: 167-171.

- [5] Maxwell, J.C. (1904). *A Treatise on Electricity and Magnetism*, 2<sup>nd</sup> ed. Oxford University Press, Cambridge, UK.
- [6] Koo, J. and Kleinstreuer, C. (2004). A new thermal conductivity model for nanofluids. *Jour. Nanoparticle Res.* 6: 577-588.
- [7] Koo, J. and Kleinstreuer, C. (2005). Laminar nanofluid flow in microheat-sinks. *Intl. J Heat Mass Transfer.* 48: 2652-2661.
- [8] Murshed, S.M.S., Leong, K.C. and Yang, C. (2005). Enhanced thermal conductivity of TiO<sub>2</sub>-water based nanofluids. *Intl. Jour. Thermal Sciences.* 44: 367-373.
- [9] Hamilton, R.L. and Crosser, O.K. (1962). Thermal conductivity of heterogeneous two-component system. *I and EC Fundamentals.* 1: 187-191.
- [10] Bruggemen, D.A.G. (1935). Berechnung Verschiedener Physikalischer Konstanten von Heterogenen Substanzen, I. Dielektrizitätskonstanten und Leitfähigkeiten der Mischkörper aus Isotropen Substanzen. *Annalen der Physik. Leipzig.* 24: 636–679.
- [11] Prasher, R., Bhattacharya, P. and Phelan, P.E. (2006). Brownian-motion-based convective-conductive model for the effective thermal conductivity of nanofluids. *Jour. Heat Transfer.* 128: 588-595.
- [12] Jang, S.P. and Choi, S.U.S. (2007). Effects of various parameters on nanofluid thermal conductivity. *Jour. Heat Transfer.* 129: 617- 623.
- [13] Li, C.H., Williams, W., Buongiorno, J., Hu, Lin-Wen and Peterson, G.P. (2008). Transient and steady-state experimental comparison study of effective thermal conductivity of Al<sub>2</sub>O<sub>3</sub>/water nanofluids. *Jour. Heat Transfer.* 130 (4): 042407.
- [14] Wang, X.-Q. and Mujumdar, A.S. (2007). Heat transfer characteristics of nanofluids: a review. *Intl. Jour. of Thermal Sciences.* 46: 1-19.
- [15] Alfa Aesar. 2008. Available: <http://www.alfaesar.com>. Last accessed April 15, 2008.
- [16] Xuan, Y., Li, Q. and Hu, W. (2003). Aggregation structure and thermal conductivity of nanofluids. *AIChE Journal.* 49(4): 1038-1043.
- [17] P.A. Hilton. (2005). *Experimental operating and maintenance procedures for thermal conductivity of liquids and gases unit.* P.A.Hilton Ltd., Hampshire, England.
- [18] Incropera, F.P. and DeWitt, D.P. (1996). *Introduction to Heat Transfer.* 3<sup>rd</sup> ed. John Wiley & Sons, Inc., New York.
- [19] Coleman, H.W. and Steele, W.G. (1999). *Experimentation and uncertainty analysis for engineers.* 2<sup>nd</sup> ed. John Wiley & Sons Inc., New York.

- [20] Omega Engineering Inc. (2005). *The Data Acquisition Systems Handbook*. Stamford, CT.
- [21] ASHRAE. (2005). *ASHRAE Handbook – Fundamentals (SI)*. American Society of Heating, Refrigerating and Air-Conditioning Engineers Inc., Atlanta. 21.4-21.7.

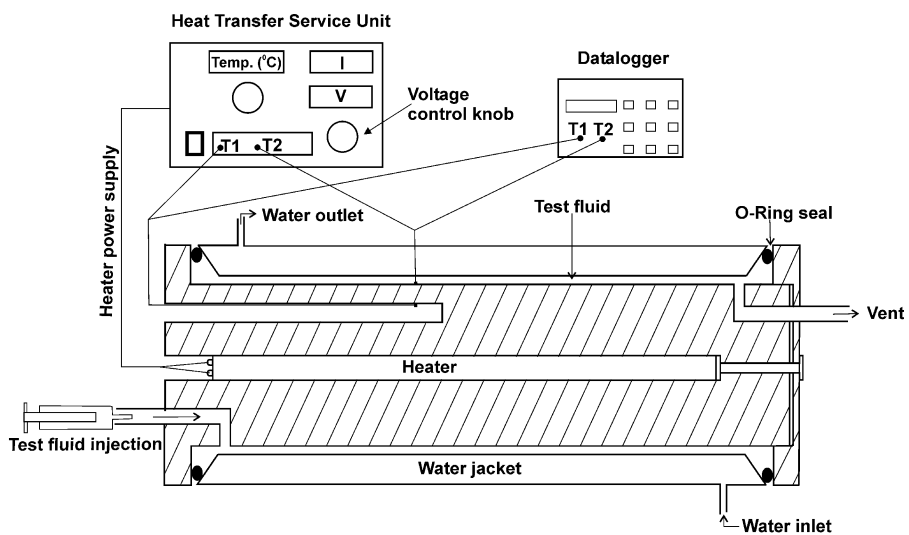


Figure 4.1 Experimental setup for thermal conductivity measurements of SiO<sub>2</sub> nanofluid.

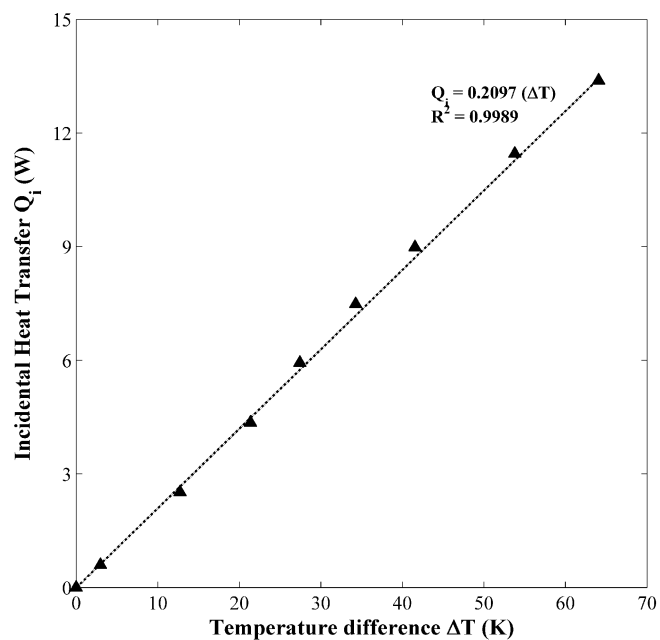


Figure 4.2 Calibration curve for the incidental heat transfer using air as the test fluid.

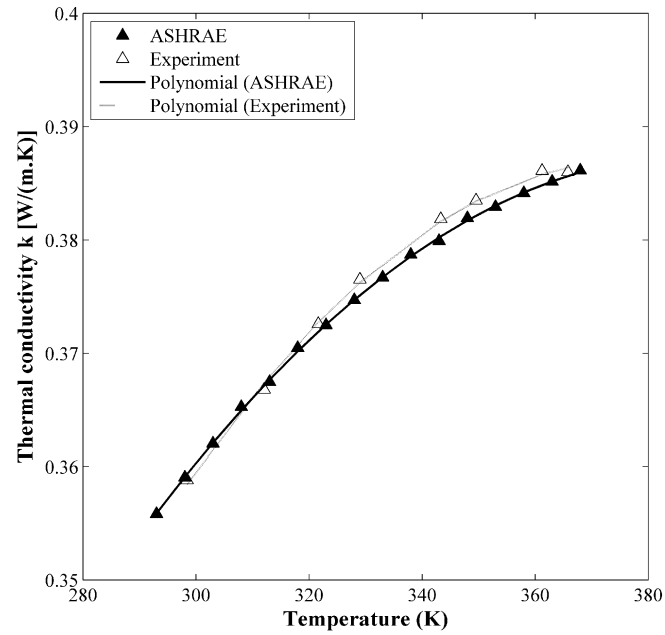


Figure 4.3 Benchmark test case to compare measured thermal conductivity values with the ASHRAE data for 60:40 EG/W.

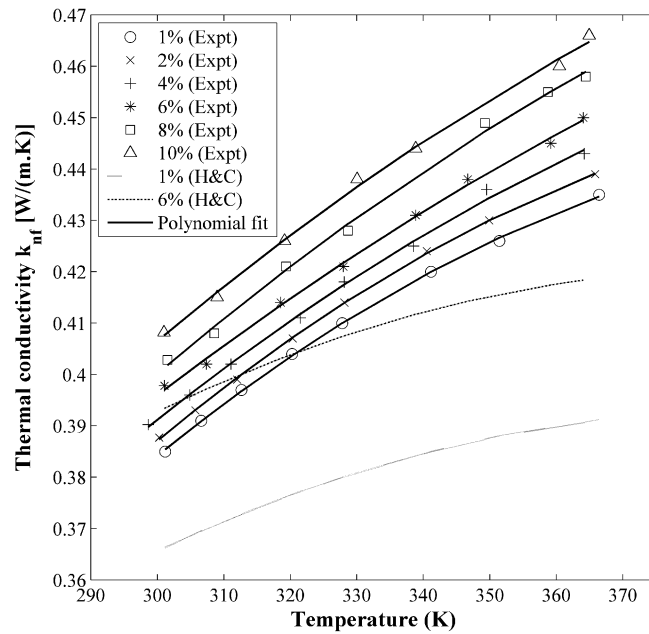


Figure 4.4 Variation of thermal conductivity with temperature for several concentrations of  $\text{SiO}_2$  nanofluid and comparison with the Hamilton-Crosser (H&C) model.

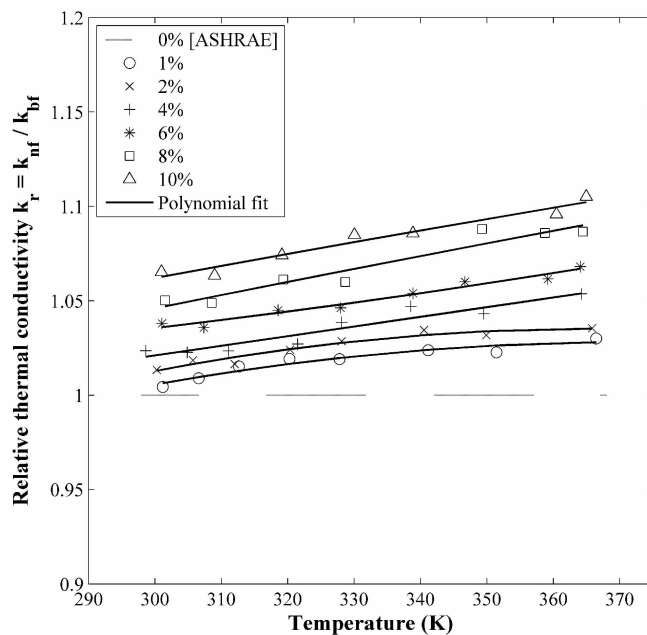


Figure 4.5 Variation of thermal conductivity ratio with temperature for different volumetric concentrations of SiO<sub>2</sub> nanofluid.

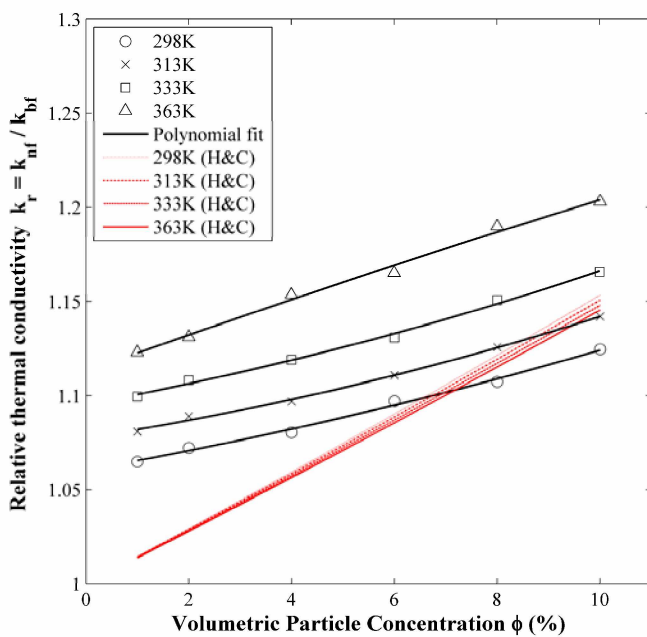


Figure 4.6 Variation of thermal conductivity ratio with concentration for SiO<sub>2</sub> nanofluid from experiment and Hamilton-Crosser correlation (H&C).

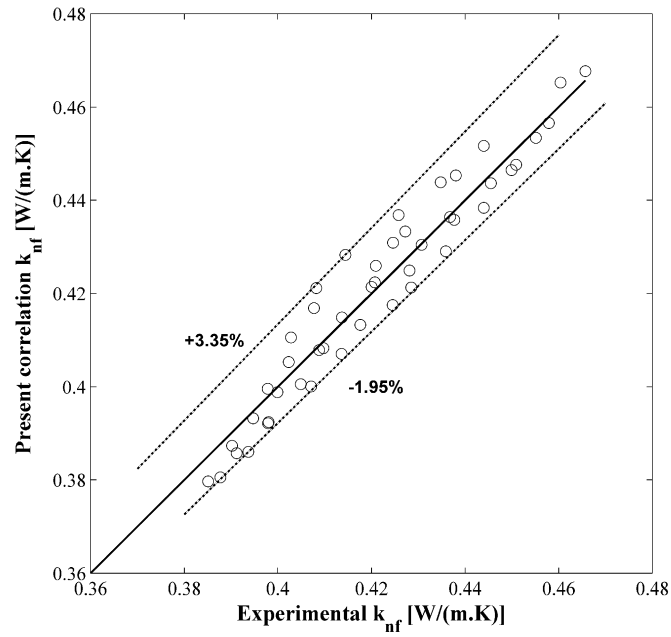


Figure 4.7 Comparison of experimental thermal conductivity with predicted values for SiO<sub>2</sub> nanofluid obtained from the new correlations [Eqs 9(a)-(c)].

## CHAPTER 5

### FREEZE-THAW CHARACTERISTICS OF WATER-BASED COPPER OXIDE NANOFLUID<sup>1</sup>

#### **Abstract**

This research is aimed at examining the freeze-thaw characteristics of a water-based copper oxide nanofluid for its successful application in cold regions, where freezing of heat transfer fluids is possible. Experiments were conducted to determine the effects of freezing on the average particle size (APS) of nanofluid suspensions due to agglomeration. Furthermore, the effect on the freezing point of the base fluid due to the addition of nanoparticles up to a volumetric concentration of 5 percent was studied. Another objective was to examine the freezing rate to determine if a nanofluid freezes faster than its base fluid. The measurements show that the APS is larger after freezing and the addition of nanoparticles does not affect the freezing point of the nanofluid at the concentrations tested. It was observed that the nanofluid freezes faster than the base fluid. When the particle concentration is higher, the nanofluid freezes at a faster rate.

**Keywords :** Nanofluid, particle size, freeze-thaw, copper oxide, freezing point

#### **1. Introduction**

Nanofluids are dispersions of nano-scale particles (e.g. copper oxide, aluminum oxide and silicon dioxide etc.) suspended in conventional heat transfer fluids such as water, ethylene or propylene glycol. Nanofluids have shown to have greater thermal conductivity than the base fluids without the nanoparticles. This enhancement of thermal conductivity increases the convective heat transfer coefficient. The laws of heat transfer dictate that a fluid with high thermal conductivity would greatly enhance the efficiency of heat exchangers. In cold regions, the hydronic heating coils are extensively used as heat exchangers for building heating as described by McQuiston et al. (2000). Automobiles require heat transfer fluid to serve as engine coolant. Therefore, nanofluids are potential candidates for heat transfer applications. In extreme cold climates, nanofluids in automobile radiators or heating coils of a building, where the heating system has failed, are susceptible to freezing.

---

<sup>1</sup> Manuscript under preparation

Presently, the main challenge for nanofluid to become an efficient heat transfer fluid is to achieve stable suspensions over a considerable period of time. To the best of our knowledge, no reliable data is available on the effect of freezing on the particle size. In other words it is not known if there is any agglomeration of nanoparticles transforming them to microparticles due to freezing. Hong and Marquis (2007) stated that agglomeration leads to change in thermal properties of the nanofluids, because the nanoparticles gradually separate from the base fluid. Many models including those of Chon et al. (2005), and Koo and Kleinstreuer (2004) show that as the particle size increases, the thermal conductivity of nanofluids decreases. Boutine (2001) reported that nanoparticles have about 20 % of their atoms near the surface, facilitating the transfer of heat efficiently. On the other hand, microparticles have most of their atoms far beneath the surface, where they are unable to transfer heat efficiently. Therefore, if the agglomeration of nanoparticles leads to the formation of microparticles, then the efficiency of heat transfer of nanofluids will diminish. Smaller nanoparticle size results in greater surface area for the same concentration and hence increased heat transfer. In cold region applications, nanofluids may undergo one or more freeze-thaw cycles and it is desirable to study the effect of such cycles on agglomeration in terms of particle size. From their research on freezing of nanofluids, prepared from carbon nanotubes in an antifreeze coolant, Hong and Marquis (2007) presented that inclusion of nanoparticles lowered the freezing point of the base fluid. The carbon nanotubes are cylindrical in shape with a high aspect ratio. They possess much higher thermal conductivity in the axial direction, in comparison to the radial direction. However, nanoparticles are quite different from the nanotubes and no similar research has been undertaken on nanoparticles in liquids. Therefore, it is desirable to conduct a freeze-thaw experiment with standard nanoparticles, which are approximately spherical in shape, with an aspect ratio of nearly unity and do not possess directional thermal conductivity.

Another property influencing the freezing of nanofluids is its thermal diffusivity. It is defined as  $\alpha = k/\rho c_p$  where  $k$  is the thermal conductivity,  $\rho$  is the density and  $c_p$  is the specific heat of the fluid. With an increase in the volumetric concentration of nanoparticles, the thermal diffusivity of a nanofluid increases. The higher the thermal diffusivity, the faster is the propagation of heat in the medium. Therefore, from the theoretical viewpoint, nanofluids will freeze faster than the corresponding base fluid. This effect needs to be verified by experiment.

Freezing and thawing characteristics of single phase fluids have been discussed extensively by Lunardini (1981). However, the freeze-thaw characteristics of nanofluids have not been investigated to understand the phenomena properly.

Therefore, the objectives of this research are to answer the following: (1) Do nanofluids freeze faster than the base fluids? Secondly, what effect does concentration have on freezing rate of nanofluids? (2) Does addition of nanoparticles lower the freezing point of nanofluids? (3) Do nanoparticles agglomerate due to the freezing? This is to be determined from particle size measurements before and after the freeze-thaw cycle?

## 2. Experimental Setup and Procedure

The original nanofluid was procured from Alfa Aesar (2008) as a 50% (by mass) aqueous suspension of copper oxide (CuO) nanoparticles, having an average particle size (APS) of 29nm. Diluted suspensions of 1% and 5% (by volume) of the nanofluid were prepared from the original nanofluid and the newly prepared samples were sonicated in a Branson B-22 (Branson, 2008) ultrasonicator for 1 hour 30 minutes to break agglomerated particles formed due to the gravitational settling. The sonicated nanofluid in a laboratory beaker of 500 ml capacity was placed inside the Thermotron 3800 Programmable Temperature chamber (Thermotron, 2008) with the ambient temperature set to  $-10^{\circ}\text{C}$ . The beaker was insulated from the top and bottom to ensure radial freezing of the nanofluid. The experimental setup is shown in Figure 1. Twenty-nine (29) copper-constantan thermocouples, distributed along two diametric cross-sections (AA' and BB'), were immersed in the nanofluid. The thermocouples were connected to a National Instruments Inc. (National Instruments, 2008a) data logger and temperature data was collected at every 15-second interval through the Labview (National Instruments, 2008b) software.

Two volumetric concentrations of the CuO nanofluid were used in this research (i.e. 1% and 5%) along with the base fluid (water). The nanofluid was frozen for nearly 14 hours and then left to thaw at room temperature for another 24 hours. Temperature data was collected by the data logger for the complete freeze-thaw cycle.

The average particle sizes of the nanofluids (both concentrations) were measured by the Dynamic Light Scattering (DLS) method using a Zeta Potential Analyzer provided by the Brookhaven Instruments Corp (Brookhaven, 2004). The apparatus was calibrated using the standard aqueous suspension of monodisperse polymer spheres provided by the National Institute of Standards and Technology (NIST). Three samples of slightly different concentration were used

and five readings for each sample were taken to obtain the final APS. The calibration results showed an APS of 99.9 nm with a standard deviation ( $\sigma$ ) of 2.6 nm, which is very comparable to the NIST certified APS of  $92 \pm 3.7$  nm with  $\sigma = 7.0$  nm.

### 3. Results

#### 3.1 Freezing Temperature and Rate

Freezing characteristic curves of deionized water and the CuO nanofluid (of 1% and 5% volumetric concentration) at the thermocouple B2 (the second one from the periphery) are shown in Figure 2. The data in this figure show that all three liquids freeze at about 0 °C. Unlike the results of Hong and Marquis (2007) with carbon nanotubes in ethylene glycol, we noticed no depression in the freezing point of the base fluid (water) due to the addition of CuO nanoparticles. The slight variation of 0.1 °C to 0.2 °C in the freezing point is within the precision of Omega type-T (copper-constantan) thermocouple, which is  $\pm 0.6$  °C.

It is observed that the rate of freezing is faster in case of the nanofluids than water. Also, the nanofluid of 5% concentration freezes faster than the nanofluid of 1% concentration. Starting from a reference temperature of 2 °C during the freezing process, while the 5% nanofluid freezes in 18.7 minutes, the 1% nanofluid and water freeze at 40.5 and 53.1 minutes, respectively. For the nanofluid of 5% concentration, the freezing continues from 18.7 minutes to about 142 minutes, when all the liquid is frozen. Then the frozen mass diminishes in temperature to -10 °C. Similar behavior was noticed at other thermocouple locations. The time-lag in freezing can be explained by a difference in thermal diffusivity of the fluids. Thermal diffusivity of higher concentration nanofluids is greater than that of a low concentration nanofluid and water. Therefore, the 5% nanofluid freezes first followed by the 1% nanofluid and water, in that order.

When the nanofluid freezes steadily towards the center there must be convection currents present in the liquid region, promoting the transfer of heat from the liquid to the frozen boundary. However, after the entire liquid column has frozen, the heat transfer from the core region to the surrounding is by pure conduction. For the 5 % nanofluids, for example, this occurs beyond 142 minutes as observed in Figure 2.

Faster freezing is a disadvantage of nanofluids, because in case of a heating system failure at subzero temperatures, pipes carrying heat transfer fluids will freeze rapidly causing bursting of pipes, damage of control valves and circulators and other problems described in the

American Society of Heating, Refrigerating and Air-Conditioning Engineers handbook (ASHRAE, 2005).

Figure 3 shows the freezing characteristic curves of deionized water obtained from four thermocouples at B1, B3, B5 and the center. Time lags are observed between the freezing temperatures recorded at thermocouple locations moving inwards along the radius. The central part of the fluid froze the last. Also, the rate of cooling was steeper for thermocouples closer to the center. This is due to the fact that as the freezing front proceeds inward, there is lesser volume of liquid left whose latent heat of freezing can be extracted in a shorter period of time.

### *3.2 Freeze-Thaw Cycle*

Figures 4 and 5 show the complete freeze-thaw characteristic curves for CuO nanofluid of 1% and 5% concentrations respectively. The freezing behavior of the nanofluids is similar to that of water. However, the rate of freezing is faster for nanofluids than for water. The thawing process exhibits a reverse trend to the freezing characteristics of nanofluids. From both the figures, different rates of freezing and thawing are noticed at the same thermocouple during the complete freeze-thaw cycle. This is due to the differing boundary conditions of  $-10^{\circ}\text{C}$  during the freezing and  $25^{\circ}\text{C}$  during the thawing process.

### *3.3 Particle Size Measurement*

The average particle sizes of the nanoparticles were measured with the DLS method and the results are summarized in Table 1 for nanofluid samples collected before and after the freeze-thaw cycle. Three samples were collected for both the unfrozen (i.e. before freezing) and thawed (after the freeze-thaw cycle was completed) nanofluid. While the unfrozen samples were collected from the ultrasonicated nanofluid, the thawed samples were collected (i) from the bottom of the beaker, (ii) middle of the beaker and (iii) from the top portion (by decantation). Five readings were taken for each sample and the software produced the combined final result. Although the APS of nanoparticles for both the concentrations are comparable with each other (148 and 164 nm for 1% and 5% concentrations, respectively), they are much higher than the manufacturer-specified size of 29 nm. This may be attributed to the agglomeration of the highly concentrated original nanofluid over a period of nearly one year from the date of procurement. Agglomeration due to a single freeze-thaw cycle increases the APS to about 240 nm, which is about 50% of the unfrozen sample. It will be a valuable study in the future to subject the nanofluid to multiple freeze-thaw cycles and find out if the APS is increasing. Then one can

subject the thawed nanofluid to ultrasonication to determine if the agglomerated nanoparticles break down to the pre-freeze average particle size.

#### 4. Conclusions

Freeze-thaw characteristics of 1% and 5% volumetric concentrations of the copper oxide nanofluid in water were studied via experiments. Results showed no lowering of the freezing point of the nanofluid due to the addition of nanoparticles. Freezing rates were found to be faster for higher volumetric concentration of nanoparticles. Concentration did not seem to affect agglomeration significantly over a single freeze-thaw cycle. Agglomeration due to a single freeze-thaw cycle increases the APS by about 50% of the unfrozen sample. Change in particle size may be studied in more detail by considering multiple freeze-thaw cycles. Ultrasonication may prove useful in breaking of bigger nanoparticles and hence result in efficient recycling of nanofluids in thermal applications.

#### Acknowledgements

The assistance of Prof. Thomas Trainor of the Chemistry Department in the use of DLS apparatus and Prof. Rorik Peterson of the Mechanical Engineering Department in the use of Thermotron Programmable Temperature chamber is gratefully acknowledged.

#### References

- Alfa Aesar. (2008). Available: <http://www.alfaesar.com>. Last accessed April 15, 2008.
- ASHRAE. (2005). *ASHRAE Handbook – Fundamentals (SI)*. American Society of Heating, Refrigerating and Air-Conditioning Engineers Inc., Atlanta. 21.4-21.7.
- Boutin, C. (2001). Taking the heat off: Nanofluids promise efficient heat transfer. *Logos*. 19(2).
- Branson Ultrasonics Corp. (2008). Available: <http://www.bransonic.com/literature.asp>. Last accessed October 18, 2008.
- Brookhaven Instruments Corporation. (2004). *90 Plus Size Analyzer*. Available: <http://www.bic.com/90Plus.html>. Last accessed: October 15, 2008.
- Chon, H.C., Kihm, K.D., Lee, S.P. and Choi, S.U.S. (2005). Empirical correlation finding the role of temperature and particle size for nanofluid ( $\text{Al}_2\text{O}_3$ ) thermal conductivity enhancement. *Appl. Phys. Letters*. 87 (153107): 1-3.

- Hong, H. and Marquis, F.D. S. (2007). *Carbon nanoparticle-containing hydrophilic nanofluid*. United States Patent Application Publication, Pub. No.:US 2007/0158610 A1.
- Koo, J. and Kleinstreuer, C. (2004). A new thermal conductivity model for nanofluids. *Jour. Nanoparticle Res.* 6: 577-588.
- Lunardini, V.J. (1981). *Heat transfer in cold climates*. Van Nostrand Reinhold Co., New York.
- McQuiston, F.C., Parker, J.D. and Spitler, J.D. (2000). *Heating Ventilating and Air-Conditioning*. John Wiley & Sons Inc., New York.
- National Instruments. (2008a). Available: <http://www.ni.com/>. Last accessed: October 5, 2008.
- National Instruments. (2008b). *Introduction Labview*. Available: <http://www.ni.com/labview>. Last accessed: October 10, 2008.
- Thermotron Benchtop Temperature Chambers. (2008). Available: <http://www.thermotron.com/products/benchtop.html>. Last accessed November 1, 2008.

Table 5.1 Average particle size distribution for the CuO nanofluid before and after freezing.

Sample	Average Particle Size (nm)	Standard Deviation (nm)
1% Before freezing	147.6	3.6
5% Before freezing	163.8	1.4
1% After freezing	223.2	1.6
5% After freezing	239.1	3.7

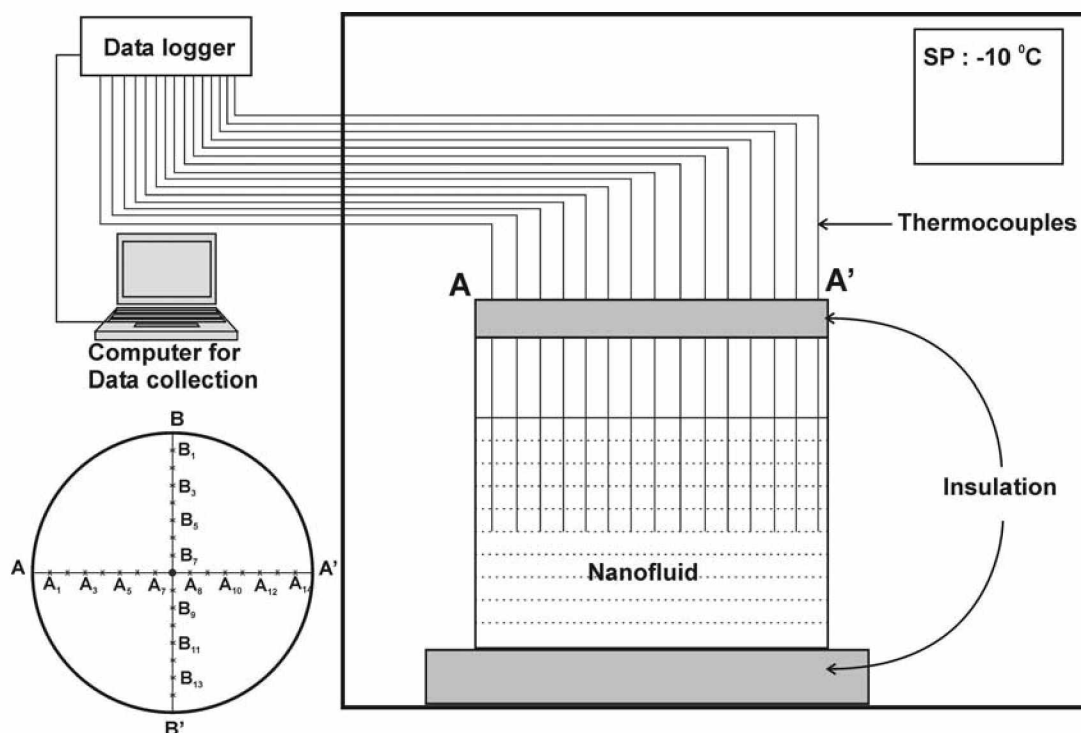


Figure 5.1 Experimental setup to study the freeze-thaw characteristics of the CuO nanofluid. Notations  $A_i$  and  $B_i$  represent locations of 29 copper-constantan thermocouples.

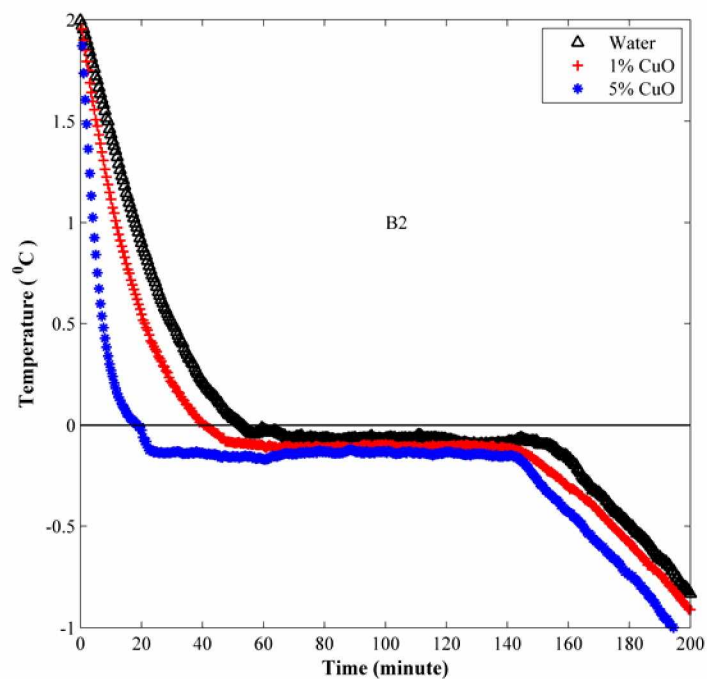


Figure 5.2 Freezing characteristic curves for water and CuO nanofluid at location B2.

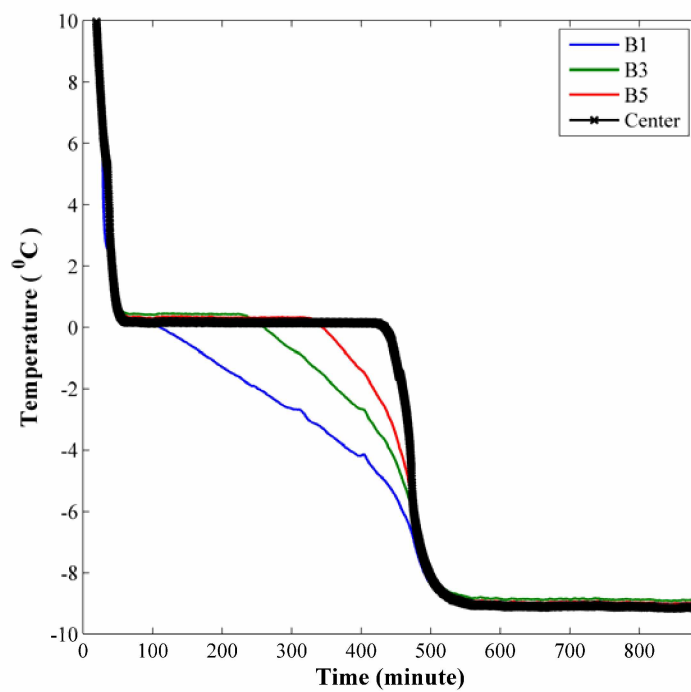


Figure 5.3 Freezing characteristic curve of deionized water.

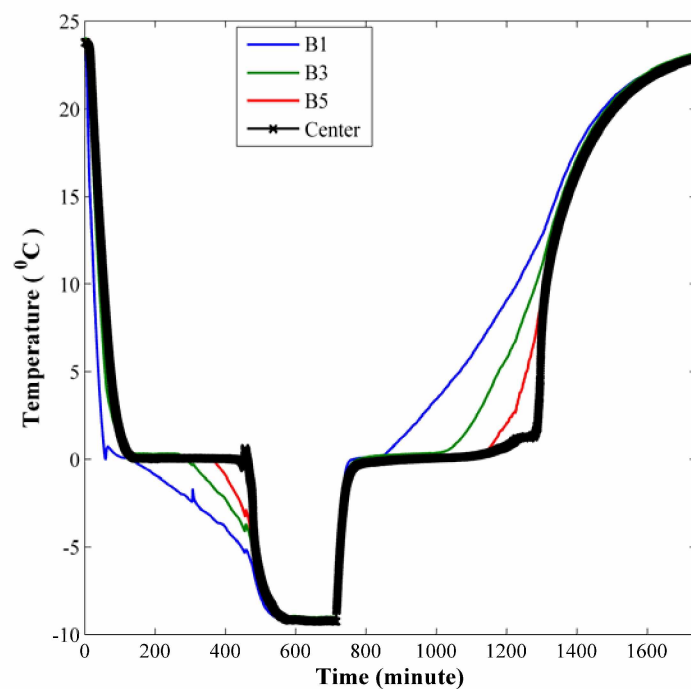


Figure 5.4 Freeze-Thaw characteristic curve of CuO nanofluid of 1% volumetric concentration.

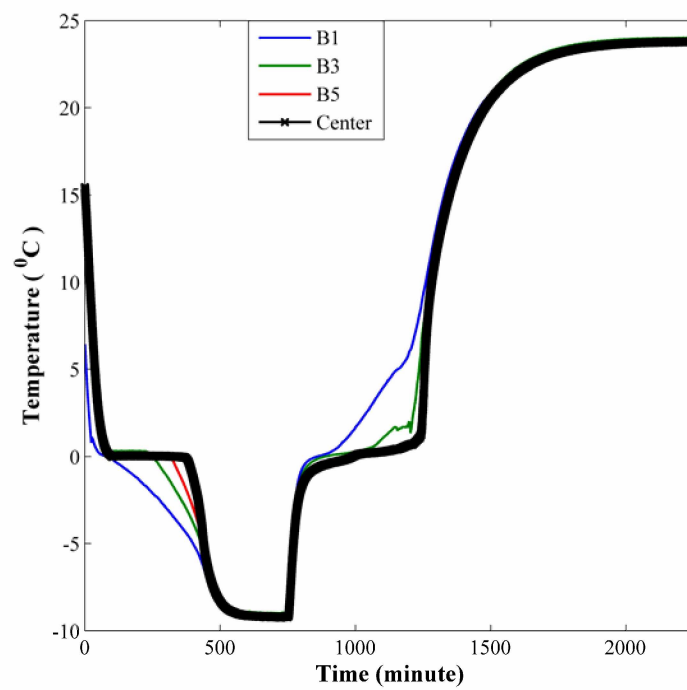


Figure 5.5 Freeze-Thaw characteristic curve of CuO nanofluid of 5% volumetric concentration.

## CHAPTER 6

### CONCLUSIONS

This thesis comprises of the study of the rheological and thermal properties and freeze-thaw characteristics of various nanofluids. Several conclusions can be drawn from the chapters presented in this thesis.

1. Aluminum oxide nanoparticles in a 60:40 EG/W base fluid exhibit a nonnewtonian behavior at a lower temperature range of 238K to 273K for all particle concentrations. It behaves as a Bingham plastic with a small yield stress, which decreases with a decrease in the volumetric concentration and an increase in fluid temperature.
2. In the higher temperature range (273K to 363K), the nanofluid behaves as a newtonian fluid.
3. The viscosity of nanofluids increases with an increase in particle concentration. For example, the viscosity of a 10% concentration aluminum oxide nanofluid is about 4 times the value of that of the base fluid at 238K.
4. Two empirical correlations have been developed to accurately determine the viscosity for two temperature regimes. In both regimes, as the temperature increases, nanofluid viscosity decreases exponentially.
5. An exponential relationship between the viscosity and volume concentration for the  $\text{Al}_2\text{O}_3$  nanoparticles in a 60:40 EG/W base fluid was observed.
6. The comparison of measured specific heat data with existing correlations showed that none of them predict specific heat accurately. From the experimental data, a new correlation was developed for the specific heat of ZnO nanofluid. This correlation is much simpler than the existing correlations and predicts specific heat of ZnO nanofluid within  $\pm 5\%$  of the measured values.
7. Thermal conductivity values for the non-metallic  $\text{SiO}_2$  nanofluid were obtained from careful experimental observations over a temperature range of 298 K to 365 K, over which the fluids in building heating systems operate. The particle volumetric concentrations ranged from 1% to 10% in a 60:40 EG/W base fluid. Thermal conductivity increased with both temperature and concentration. Existing thermal conductivity models for suspensions failed to predict the thermal conductivity of  $\text{SiO}_2$  nanofluid.

8. The Hamilton-Crosser model does not account for the effect of temperature and concentration on thermal conductivity enhancement properly. A set of new correlations was proposed by improving the Koo and Kleinstreuer model, using the experimental data collected over a broader range of temperature and concentrations than their range of validity. These new correlations predict thermal conductivity of SiO<sub>2</sub> nanofluids with a maximum deviation of 3.35% from the experimental values. Also, it is observed that nanofluids exhibit superior thermal conductivity at higher temperatures and hence their application at high temperatures may be preferable.
9. Freeze-thaw characteristics of 1% and 5% volumetric concentrations of the copper oxide nanofluid in water were studied from experimental results. Results showed no lowering of freezing point of the nanofluid due to the addition of nanoparticles. The freezing rate was faster for nanofluids than the base fluid and the freezing rates were faster for higher particle volumetric concentration. Concentration did not seem to affect agglomeration significantly over a single freeze-thaw cycle. The average particle size increased due to freezing.

Change in particle size should be studied in more detail by considering multiple freeze-thaw cycles. Ultrasonication may prove useful in the breaking of bigger nanoparticles and hence result in efficient recycling of nanofluids in thermal applications.